8-2022

Study of Single-Photon Wave-Packets with Atomically Thin Nonlinear Mirrors

Christopher Klenke
University of Arkansas, Fayetteville

Study of Single-Photon Wave-Packets with Atomically Thin Nonlinear Mirrors

A thesis submitted in partial fulfillment
of the requirements for the degree of
Master of Science in Microelectronics-Photonics

by

Christopher Klenke
Missouri State University
Bachelor of Science in Physics, 2019
Bachelor of Science in Mathematics, 2019

August 2022
University of Arkansas

This thesis is approved for recommendation to the Graduate Council.

Julio Gea-Banacloche, Ph.D.
Dissertation Director

Hugh Churchill, Ph.D.
Committee Member

Morgan Ware, Ph.D.
Committee Member

Matthew Leftwich, Ph.D.
Ex-Officio Member

The following signatories attest that all software used in this thesis was legally licensed for use by Chris Klenke for research purposes and publication.

Christopher Klenke, Student

Dr. Julio Gea-Banacloche, Thesis Director

This thesis was submitted to http://www.turnitin.com for plagiarism review by the TurnItIn company's software. The signatories have examined the report on this thesis that was returned by TurnItIn and attest that, in their opinion, the items highlighted by the software are incidental to common usage and are not plagiarized material.

Dr. Matt Leftwich, Program Director

Dr. Julio Gea-Banacloche, Thesis Director

Abstract

A novel controlled phase gate for photonic quantum computing is proposed by exploiting the powerful nonlinear optical responses of atomically thin transition metal dichalcogenides (TMDs) and it is shown that such a gate could elicit a π-rad phase shift in the outgoing electric field only in the case of two incident photons and no other cases. Firstly, the motivation for such a gate is developed and then the implementation of monolayer TMDs is presented as a solution to previous realization challenges. The single-mode case of incident photons upon a TMD is derived and is then used to constrain the more general multimode case, where the probability of producing a nonlinear response is approximated and evaluated for the tuning of various physical parameters within the system. The implications of the variability of these parameters are then discussed.

Acknowledgements

I would like to thank both of my parents for the undying and unfaltering support they have shown me over the years. I will always be grateful.

I would like to thank Dr. Julio Gea-Banacloche for his patience, his ideas, and for taking a chance on me as an overly ambitious undergraduate student. It goes without saying, but is worth saying anyways, that none of this work would be possible without his tutelage. He has helped me learn more about optics, mechanics, and Fourier transforms than I knew there was to learn. Thank you Dr. Gea-Banacloche.

I would like to thank Dr. Rick Wise for taking a chance on me as an REU student and for making my work in the Microelectronics-Photonics department possible, as well as my continued position. I would also like to thank Dr. Matt Leftwich for his guidance during some challenging moments as well as his thoughtfulness of my opportunities. I would also like to thank Renee Hearon for her calling me to help me keep my submissions and red tape together, as well as bringing my soup and tea when I was sick. Thank you all for your kindness.

Lastly, I would like to the University of Arkansas Physics Department for their financial support through continuous teaching assistantship opportunities during my research. Their efforts to ensure funding for many graduate students have been tremendous and are greatly appreciated.

Table of Contents

List of Figures

Chapter 1: General Dual-Rail Quantum Logic

1.1 Introduction

Quantum information science is based upon the idea that information can be encoded into, manipulated within, and extracted from individual quantum systems, or qubits. The individual behaviors and interactions of quantum systems, as governed by quantum mechanics, enables a mathematical computational framework that suggests advances to algorithm resource efficiency, communication security, and information storage beyond the scope of classical computers. It has spawned intricate subdisciplines like quantum cryptography and quantum communication, while pushing the known limits of physics, chemistry, electronics, and photonics to construct such qubits. Quantum information science is both deep and rich, spurring researchers to ask new questions and envision new paradigms that reveal further the fundamental secrets of Nature.

The fundamental logic component in quantum information is the qubit. A qubit is a quantum system that, at minimum, achieves five objectives: be able to be arranged into a specified initial state, preserve its quantum state properties, evolve predictably across physical operators, produce measurable, reliable results detailing the state of the system, and, lastly, be scalable (1). Many types of useful qubits exist or have been theorized, including cold ion traps, nuclear magnetic resonance (NMR), and superconducting entangled charges, as well as photons. Each type of qubit presents different advantages and disadvantages that result in tradeoffs in the five objectives, constraining their applications and reliability.

In gate-based quantum computing, logic gates are the physical operators that predictably evolve the state of a system over time and are at the center of quantum computing. There exist single-qubit gates and multiqubit gates, both of which must be represented as a unitary matrix in quantum matrix mechanics to enact any state change upon a qubit. Single-qubit gates are any physical operations that alter the probability amplitudes and phase of an individual qubit in a nontrivial way and are usually well-established and readily constructed. Multiqubit logic gates, meanwhile, are composed of single- and multiqubit operations that can reliably alter the state of one qubit in a predictable manner that depends upon the state of another qubit. In this thesis, the physical constraints of a specific photonic multiqubit operation are analyzed and then interpreted for realization in a universal multiqubit gate.

1.2 Optical Controlled NOT Gate

Photonic qubits provide convincing justification over other options. Photons have neither mass nor charge and so interact weakly with most matter and other photons, maintaining states of quantum coherence even at room temperature. They also exhibit a plethora of unique quantum behaviors in the macroscopic limit that other quantum systems do not, like the interference of the double-slit experiment or the photoelectric effect, which allow for rich information reading from even small quantities of photons. Compared to other qubits, light is mostly well-understood and well-controlled; accurately registering information into and retrieving it from electromagnetic waves is a process performed in devices ranging from satellites to television remotes.

This thesis is concerned with a qubit obtained via dual-rail encoding, where a single-photon wavepacket is incident upon a nonpolarizing beam splitter with splitting angle 45°. Two low-loss optical waveguide fibers are placed opposite the splitter, one in the transmitted mode and one in the reflected mode, and the photon enters a Fock state occupying a superposition of the two fibers. Its wavefunction is defined as

$$|\Psi\rangle = c_1|0\rangle + c_2|1\rangle, \qquad \text{(Equation 1.1)}$$

where, in the computational ($|0\rangle$,$|1\rangle$) basis, c_1 (c_2) is the probability amplitude of an electric field excitation being in the first (second) fiber mode and the vacuum state in the second (first) mode.

Each amplitude represents a $|c_1|^2$ or $|c_2|^2$ chance of the photon existing in its respective fiber. The amplitude coefficients, α and β, are both dependent on the angle of the beam splitter but combined they give a guaranteed chance to be measured in either fiber, hence the summation constraint

$$|c_1|^2+|c_2|^2=1. \qquad \text{(Equation 1.2)}$$

In vector form, Equation 1.1 is represented as

$$|\Psi\rangle=\begin{pmatrix}c_1\\c_2\end{pmatrix}, \qquad \text{(Equation 1.3)}$$

while the measurement states themselves are

$$|0\rangle=\begin{pmatrix}1\\0\end{pmatrix},$$

$$|1\rangle=\begin{pmatrix}0\\1\end{pmatrix}. \qquad \text{(Equation 1.4)}$$

This corresponds, notationally, to the photon being observed in the fiber pre-designated as the $|1\rangle$ or $|0\rangle$ state, respectively.

A two-qubit system extends the Hilbert space dimensionality of the single qubit manifold to the basis

$$|\psi_1\rangle \otimes |\psi_2\rangle = \begin{pmatrix}\alpha_1\\ \beta_1\end{pmatrix} \otimes \begin{pmatrix}\alpha_2\\ \beta_2\end{pmatrix} = \begin{pmatrix}\alpha_1\alpha_2\\ \alpha_1\beta_2\\ \beta_1\alpha_2\\ \beta_1\beta_2\end{pmatrix} = |\psi_1\psi_2\rangle, \qquad \text{(Equation 1.5)}$$

where α_1, β_1, α_2, β_2, obey the normality constraint defined in Equation 1.2, as well as their products do so for $|\psi_1\psi_2\rangle$. For $|\psi_1\rangle$ and $|\psi_2\rangle$ already in set states, an example of two qubits where $|\psi_1\rangle$=$|1\rangle$ and $|\psi_2\rangle$=$|0\rangle$ would take the form

$$|1\rangle \otimes |0\rangle = \begin{pmatrix}0\\ 1\end{pmatrix} \otimes \begin{pmatrix}1\\ 0\end{pmatrix} = \begin{pmatrix}0\\ 0\\ 1\\ 0\end{pmatrix} = |10\rangle. \qquad \text{(Equation 1.6).}$$

This basis is useful because the four-component vector notation assumes a concise value for each possible input state of $|\psi_1\psi_2\rangle$, with the one state occupying a different row in the column.

The universal logic gate for any qubit, including dual-rail, is the Controlled-NOT gate (CNOT), U_{CN} (2–4). This is due to ability of the U In a circuit of two qubits, the CNOT performs a logical operation upon one qubit (the target qubit) if and only if the other qubit (the control qubit) is in a specific state. A U_{CN} gate applied to the state in Equation 1.5 flips the amplitudes of the target qubit (i.e., performs a NOT operation it) resulting in

$$U_{CN}|\psi_1\psi_2\rangle = U_{CN}\begin{pmatrix}\alpha_1\alpha_2\\ \alpha_1\beta_2\\ \beta_1\alpha_2\\ \beta_1\beta_2\end{pmatrix} = \begin{pmatrix}\alpha_1\alpha_2\\ \alpha_1\beta_2\\ \beta_1\beta_2\\ \beta_1\alpha_2\end{pmatrix} = |\psi_1\psi_2\rangle'. \qquad \text{(Equation 1.7)}$$

In the computational basis this is represented with the unitary matrix

$$U_{CN} = \begin{pmatrix} 1 & 0 & 0 & 0 \\ 0 & 1 & 0 & 0 \\ 0 & 0 & 0 & 1 \\ 0 & 0 & 1 & 0 \end{pmatrix}. \qquad \text{(Equation 1.8)}$$

Continuing the example developed in Equation 1.6, an operation of U_{CN} upon $|10\rangle$ gives

$$U_{CN}|10\rangle = \begin{pmatrix} 1 & 0 & 0 & 0 \\ 0 & 1 & 0 & 0 \\ 0 & 0 & 0 & 1 \\ 0 & 0 & 1 & 0 \end{pmatrix}\begin{pmatrix} 0 \\ 0 \\ 1 \\ 0 \end{pmatrix} = \begin{pmatrix} 0 \\ 0 \\ 0 \\ 1 \end{pmatrix} = |11\rangle. \qquad \text{(Equation 1.9)}$$

It is necessary to note here that the basic algebraic structure of U_{CN} does not necessitate the flipping of the $|\psi_2\rangle$ state by the state of $|\psi_1\rangle$, it simply will only ever flip the bottom components of the $|\psi_1\psi_2\rangle$' vector state while performing an identity operation upon the top two components. Realizing this necessary controlled flip is an algorithmic accomplishment and can be achieved through the implementation the Hadamard logic gate, U_H, and the controlled-phase gate, U_{CP}.

The Hadamard gate is a compound, single-qubit unitary operation defined by the matrix

$$U_H = \frac{1}{\sqrt{2}}\begin{pmatrix} 1 & 1 \\ 1 & -1 \end{pmatrix}, \qquad \text{(Equation 1.10)}$$

where the term compound merely means that is achieved through other, more fundamental single-qubit operations. Producing a reliable, high-fidelity U_H gate in dual-rail logic is rather easy when compared to the elaborate facilities necessary for other qubits. Interferometer equipment such as mirrors, collimators, phase shifters, and quantum beam splitters are effective single-qubit operators, and, when composed together, can form any possible single-qubit gate, and thus also U_H (5).

Regarding the operations naturally performed by the phase shifters and beam splitters, a useful reformulation of Equation 1.1 is

$$|\Psi\rangle = \cos\theta\,|0\rangle + e^{i\phi}\sin\theta\,|1\rangle, \qquad \text{(Equation 1.11)}$$

with the vector form

$$|\Psi\rangle = \begin{pmatrix} \cos\theta \\ e^{i\phi}\sin\theta \end{pmatrix}. \qquad \text{(Equation 1.12)}$$

The amplitude coefficients still maintain the normalization condition in Equation 1.2. In this form, a beam splitter gate acting upon a qubit translates the qubit into annihilation and creation operations in the splitter's reflected and transmitted modes. This gate, U_B, acts upon a qubit depending upon its natural splitting angle θ, and performs the matrix

$$U_B = \begin{pmatrix} \cos\theta & -\sin\theta \\ \sin\theta & \cos\theta \end{pmatrix}. \qquad \text{(Equation 1.13)}$$

A beam splitter acting upon an existing qubit has both waveguides incident upon it, as depicted in Figure 1.1 with a splitting angle θ.

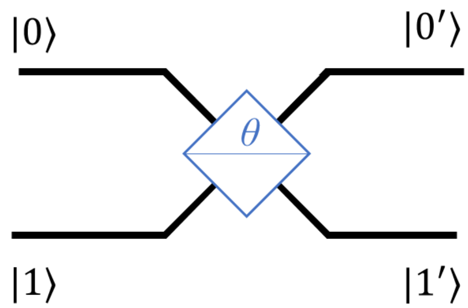

Figure 1.1 Beam Splitter Logic Gate

Often, the beam splitter used to conjure the qubit initially is of 45° to present an even likelihood of the photon appearing in either rail. However, this does not have to always be the case, and other angles may be employed later in the circuit to coax a given qubit into one state over another for a specific algorithm. An inverse beam splitter (i.e., with a negative angle) could be introduced as well to implement the opposite operation to a set of amplitudes; the use of a beamsplitter with some angle θ and then the use of another beam splitter with angle -θ simply reverts the qubit to its initial state as an identity operation.

Phase shifters, when placed within the propagation of one of the fibers, slow the time-evolution of that mode in regards the other one. The amount of phase shift produced by the shifter depends upon the refractive index of the material and the total distance a photon travels through it, but it can be reduced to general phase ϕ, and gives the gate U_P with the matrix

$$U_P = \begin{pmatrix} e^{-i\phi} & 0 \\ 0 & e^{i\phi} \end{pmatrix}. \qquad \text{(Equation 1.14)}$$

A phase shift operation is demonstrated in Figure 1.2, where only the first mode of the qubit, $|0\rangle$, interacts with a phase shifter of some phase ϕ.

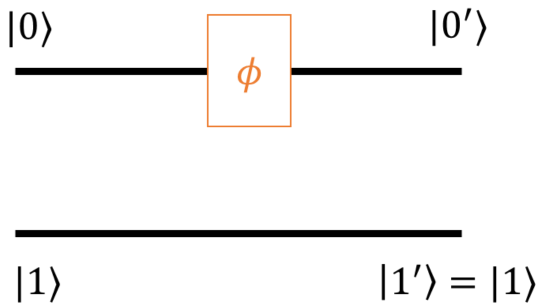

Figure 1.2 Phase Shifter Logic Gate

The U_{CP} gate, meanwhile, requires an interaction between multiple photons and cannot arise from common beamsplitters and phase shifters. To achieve a functional U_{CP}, one qubit's state (and thus, one photon's) must be able to impose an alteration on another's state. This is most often attempted with a medium possessing a strong nonlinear dielectric response. Figure 1.3 shows two qubits $|\psi_1\rangle$ and $|\psi_2\rangle$ share a combined state $|\psi_1\psi_2\rangle$. This combined state is fed into a pair of beam splitters with arbitrary angles θ_1 and θ_2 are used to arrange the photons into either its corresponding $|0\rangle$ or $|1\rangle$ state. The composite state is then either $|00\rangle$, $|01\rangle$, $|10\rangle$, or $|11\rangle$, whereupon the phase shifters of ϕ_0 and ϕ_χ act upon the qubits. The ϕ_0 shifters are set so that they are equivalent to the phase induced by ϕ_χ upon a single photon so that if the set of qubits are in the $|00\rangle$ state, they both receive an identical phase shift ϕ_0 and then lose it. If they are in the either the $|10\rangle$ or $|01\rangle$ state, again, both receive no net phase shift. However, if the set of photons is in the $|11\rangle$ state, the nonlinear response is activated in the χ medium, and both photons receive a different total phase shift ϕ of

$$\phi = \phi_\chi - 2\phi_0. \qquad \text{(Equation 1.15)}$$

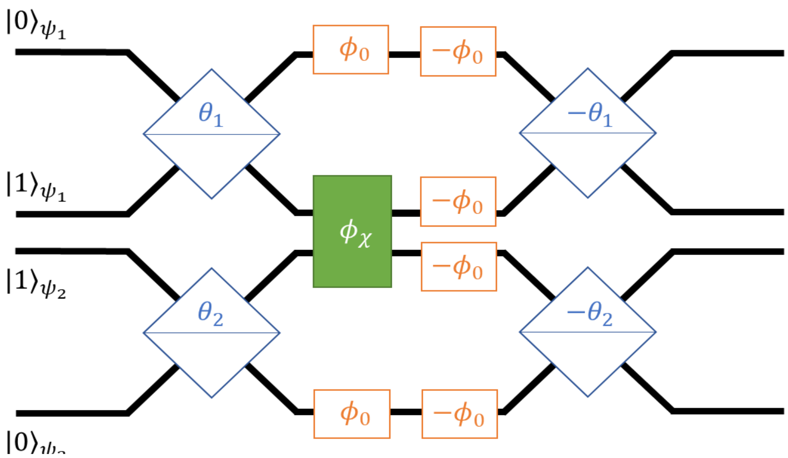

Figure 1.3 Example U_{CP} Set-up

A U_{CP} facilitated by a nonlinear medium, as depicted in Figure 1.3, performs the transformation

$$U_{CP}|00\rangle = |00\rangle,$$
$$U_{CP}|01\rangle = |01\rangle,$$
$$U_{CP}|10\rangle = |10\rangle,$$
$$U_{CP}|11\rangle = e^{i\phi}|11\rangle, \qquad \text{(Equation 1.16)}$$

which is represented as the matrix

$$U_{CP} = \begin{pmatrix} 1 & 0 & 0 & 0 \\ 0 & 1 & 0 & 0 \\ 0 & 0 & 1 & 0 \\ 0 & 0 & 0 & e^{i\phi} \end{pmatrix}. \qquad \text{(Equation 1.17)}$$

In the ideal case, $\phi = \pi$, two U_H gates can be included to develop the overall operation

$$U_H U_{CP} U_H = \frac{1}{\sqrt{2}}\begin{pmatrix}1 & 1 & 0 & 0\\ 1 & -1 & 0 & 0\\ 0 & 0 & 1 & 1\\ 0 & 0 & 1 & -1\end{pmatrix}\begin{pmatrix}1 & 0 & 0 & 0\\ 0 & 1 & 0 & 0\\ 0 & 0 & 1 & 0\\ 0 & 0 & 0 & -1\end{pmatrix}\frac{1}{\sqrt{2}}\begin{pmatrix}1 & 1 & 0 & 0\\ 1 & -1 & 0 & 0\\ 0 & 0 & 1 & 1\\ 0 & 0 & 1 & -1\end{pmatrix},$$

$$= \begin{pmatrix}1 & 0 & 0 & 0\\ 0 & 1 & 0 & 0\\ 0 & 0 & 0 & 1\\ 0 & 0 & 1 & 0\end{pmatrix} = U_{CN}, \qquad \text{(Equation 1.18)}$$

i.e., the universal quantum gate. Thus, if a realistic U_{CP} could be fabricated from nonlinear media, any quantum algorithm could be built with dual-rail qubits.

1.3 Nonlinear susceptibility and atomically thin transition metal dichalcogenides

Nonlinear optical responses occur in classical optics when the dielectric optical response properties of a given medium are modified by a sufficiently intense incident beam of light. In principle, the phenomenon scales down to the quantized radiation field level of individual photons. In condensed matter media the polarizing response to the driving field is the culprit, defined as the dipole moment per unit volume, $P(t)$. In a lossless and dispersionless medium, the induced polarization via its dielectric susceptibility expands generally as a power series of the driving electric field to (6,7)

$$P(t) \; = \; \sum_{n=\infty} \chi^{(n)} E^n(t), \qquad \text{(Equation 1.19)}$$

where $\chi^{(n)}$ is the electric susceptibility tensor of order n (also of rank n) and $E^n(t)$ is the applied electric field to the nth power.

The form of each order of χ is a proportionality tensor of rank n with physical values that arise intrinsically from the energy states and wavefunctions of the dipoles that make up the medium, and the crystal pattern symmetries. These forms can be derived analytically and predicted for a given material, but this is beyond the scope of this document and only experimental recordings are considered. The tensors also depend upon the frequency of the driving field, in general, but in a medium with sufficiently low loss and fast response the frequency dependence can be neglected. Higher-order (nonlinear) susceptibilities are often exceedingly small in comparison to the linear $\chi^{(1)}$ value and hence their negligibility in the conventional (linear) regime. Some common nonlinear crystals available from commercial providers, for example, such as $LiNbO_3$ and beta-barium borate (BBO) have second harmonic generation $\chi^{(2)}$ on the order of 1e-15m/V (8). Clearly, a high intensity beam of light is necessary to incur any measurable nonlinear response.

Fiber optic communication channels do manage to still use this phenomenon and trade information directly between light waves with the $\chi^{(3)}$ polarization response in nonlinear Kerr media. In this event, a third-order nonlinear optical response is triggered in a medium with a refractive index that varies with intensity. This intensity variation allows for the presence of one beam of light to modify (i.e., control) the phase of a second beam. While originally a promising outlet for cross-photon interactions, it has since been proven strongly (9,10) that in the paradigm of individual photons this effect cannot have useable quantum computation fidelity. This is because both photons must have such a strong interaction with the medium that they are absorbed and re-emitted numerous times throughout their propagation within it, leading to an insurmountable amount of phase noise in the qubit when collected after the operation.

Nonlinear phenomena that are stimulated by the second order term of the polarization, $\chi^{(2)}$, however, offer a promising alternative for photonic quantum gates. In recent years there has been a growing load of research in the feasibility of photon-photon interactions mediated by $\chi^{(2)}$ responses that minimize field distortions, i.e., the noise issue that precludes Kerr-based gates (11–14). By second-harmonic generation (2HG), a nonlinear medium absorbs two wavepackets of the same frequency and, upon relaxation to the ground state, emits a single wavepacket with double the frequency of the originals. This also manifests in a dual-rail set up as two qubits that each have a mode passing through the medium that triggers the nonlinear response for a U_{CP} if the photons of each qubit are in the mode of the medium simultaneously. It presents an intriguing alternative to Kerr media gates, should a sufficiently useful $\chi^{(2)}$ be realized.

Over the past decade, researching atomically thin transition metal dichalcogenides (TMDs) and their semiconductor properties has become a widely-studied subject (15–18). In 2010, monolayer MoS2 was shown to alter its 1.29 eV indirect bulk bandgap value to a 1.9 eV direct bandgap semiconductor in the monolayer regime. The behavior of converting to a direct bandgap semiconductor has since been identified in MoSe2, MoTe2, WS2, and WSe2, as well, hence the common usage of the term TMD. The source of this trend resides in the shifts of both the conduction and valence bands' minimums and maximums, respectively, across the Brillouin zone. In bulk, and in even-numbered layers of atomic thin TMD sheets, the valence band maximum occurs at the Γ point in the center of the hexagonal Brillouin zone while the conduction band minimums appear at points in between the Γ center and K points at the vertices. However, when reduced to a single layer (and for few odd-numbered layered sheets), both gaps align directly above the K points (19,20).

Additionally, the optical properties of monolayer TMDs are quite exotic. Binding energies of optically induced excitons for TMDs are regularly reported into the 100s of meVs (21,22), indicating high stability at room or higher temperature. They possess short radiative lifetimes with decay rates γ on the order of

$$\gamma \approx 1/ps \qquad \text{(Equation 1.20)}$$

result in oscillation strengths on the order of

$$f = \gamma/\omega_0 \approx 10^{-3}, \qquad \text{(Equation 1.21)}$$

where ω_0 is the exciton's natural resonance frequency. The rapid radiative decay rates and high oscillatory factor produce a strong light-matter coupling constant, g_0, that can be further enhanced in the frame of a Fabry-Pérot cavity or nearby reflector. These exciton behaviors can be attributed to trapping the exciton to an in-plane momentum along the TMD layer with the limited Coulomb screening between the hole-electron pair due to the anisotropic environment presented by the lattice structure of the TMD (22–24).

Such exciton generation and sustainment abilities lend themselves to highly nonlinear optical susceptibilities, producing a $\chi^{(2)}$ response being reported for in MoS2, MoSe2, MoTe2, WS2, and WSe2 on the order of 1e-9m/V (25–29), three orders of magnitudes higher than the best bulk nonlinear materials available today. Furthermore, advances in manipulating the optically induced excitons via surface strain, external field driving, and frequency tuning alignments suggest even greater $\chi^{(2)}$ responses (30–32). It is worth noting, however, that there is much discrepancy between maximum achieved values of the $\chi^{(2)}$ second-harmonic generation by different research groups, even for TMDs of the same chemical composition and polytype (20,33).

Monolayer TMDs have myriad exciting optoelectronic features that of interest to engineering applications at the micro and nanoscale. Their nonlinear susceptibilities, moreover, present an intriguing option for a $\chi^{(2)}$ medium to construct a useful U_{CP} for universal quantum computation. Fidelity aside, assessing the parameters of the quantum mechanical interaction between a nonlinear atomically thin TMD for both single and two photon interactions is the logical next step, and is pursued in the following chapters.

Chapter 2: Single-mode photon-TMD interaction analysis

2.1 Single-Mode Single Photon Analysis

A semiclassical thought experiment of one photon incident upon a TMD monolayer was first considered. In this situation, the cavity excitation is destroyed by the TMD upon interaction, initiating the creation of an exciton within the TMD. In a lossless and dispersionless medium, the exciton exists for some time before the electron-hole pair collapse together, emitting a new cavity excitation. This problem is treated in the Schrödinger picture as a pair of coupled quantum oscillators in an optical cavity, the first being a single-mode field excitation incident upon the mirror and the second being the atomic transition excitation (exciton) existing within the mirror. The specific relationship to be investigated is the nonlinear function χ and the natural coupling constant of the TMD between the exciton and the photon, g_0.

During this interaction, the photon-exciton interactions are governed by the Hamiltonian

$$H = g_0(ab^\dagger + ba^\dagger) + \chi b^\dagger b^\dagger bb, \qquad \text{(Equation 2.1)}$$

where a and b are the annihilation operators for the photon and exciton, respectively, and $a^\dagger$ and $b^\dagger$ are the creation operators for the photon and exciton, respectively. The χ is the short-range interaction energy of the excitons inherent to a given TMD, and the state of a single photon incident upon the system can be written as

$$|\psi(t)\rangle = C_{10}(t)|10\rangle + C_{01}(t)|01\rangle, \qquad \text{(Equation 2.2)}$$

where the $|10\rangle$ state is when one photon exists in the cavity and no excitons and $|01\rangle$ is the state of no photon and one exciton. The coefficients $C_{10}(t)$ and $C_{01}(t)$ represent the equations of motion for their respective states.

To find these equations, the time-dependent Schrödinger equation,

$$\frac{\partial}{\partial t}|\psi\rangle = -\frac{i}{\hbar}H|\psi\rangle, \qquad \text{(Equation 2.3)}$$

was applied to Equation 2.1 and Equation 2.2, developing

$$\dot{C}_{10}(t)|10\rangle + \dot{C}_{01}(t)|01\rangle = -i\frac{g_0}{\hbar}(C_{10}(t)|01\rangle + C_{01}(t)|10\rangle), \qquad \text{(Equation 2.4)}$$

where the time-derivative dot notation is introduced. Note that it is evident that the $b^\dagger$ operators in the second term of the Hamiltonian fully annihilate any potential exciton-exciton interaction, and consequently any nonlinear response from χ. This is intuitive as a nonlinear response is necessarily caused by an interaction between multiple photons. Note the relationship between g_0 and $\hbar$, and that moving forward $\hbar$ is absorbed into g_0 as a single-step unit of energy.

After congregating like states,

$$\dot{C}_{10}(t) = -ig_0C_{01}(t),$$
$$\dot{C}_{01}(t) = -ig_0C_{10}(t), \qquad \text{(Equation 2.5)}$$

the second time-derivative of $C_{10}(t)$ was found as

$$\ddot{C}_{10}(t) = -ig_0\dot{C}_{01}(t) = -ig_0\big(-ig_0C_{10}(t)\big),$$

$$\ddot{C}_{10}(t) + g_0^2C_{10}(t) = 0, \qquad \text{(Equation 2.6)}$$

and, similarly, for $C_{01}(t)$ to be

$$\ddot{C}_{01}(t) + g_0^2C_{01}(t) = 0. \qquad \text{(Equation 2.7)}$$

These have the respective general solutions

$$C_{10}(t) = Ae^{ig_0t} + Be^{-ig_0t},$$

$$C_{01}(t) = Ce^{ig_0t} + De^{-ig_0t}, \qquad \text{(Equation 2.8)}$$

with general coefficients *A*, *B*, *C*, and *D*, whose time derivatives are

$$\dot{C}_{10}(t) = Aig_0e^{ig_0t} - Big_0e^{-ig_0t},$$

$$\dot{C}_{01}(t) = Cig_0e^{igt} - Dig_0e^{-ig_0t}. \qquad \text{(Equation 2.9)}$$

Equation 2.8 was plugged-in to Equation 2.5 on the right-hand side (RHS) while Equation 2.9 was substituted into the left-hand side (LHS), producing

$$Aig_0e^{ig_0t} - Big_0e^{-ig_0t} = -ig_0\big(Ce^{ig_0t} + De^{-ig_0t}\big),$$

$$Cig_0e^{igt} - Dig_0e^{-ig_0t} = -ig_0\big(Ae^{ig_0t} + Be^{-ig_0t}\big). \qquad \text{(Equation 2.10)}$$

Arranging by like terms and then reducing gave the coefficient relationships

$$A = -C,$$
$$B = D. \qquad \text{(Equation 2.11)}$$

In this system the initial state was assumed to start with one cavity excitation and no exciton for the initial conditions. At time $t = 0$ the equations of motion were

$$C_{10}(t = 0) = 1,$$
$$C_{01}(t = 0) = 0. \qquad \text{(Equation 2.12)}$$

These can be implemented into Equation 2.8 to yield

$$A + B = 1,$$
$$C + D = 0, \qquad \text{(Equation 2.13)}$$

and at time $t = 0$, Equation 2.10 becomes

$$A - B = -(C + D)$$
$$C - D = -(A + B). \qquad \text{(Equation 2.14)}$$

The relationships in Equation 2.11, Equation 2.13, and Equation 2.14 were used to establish the exact values of the coefficients as

$$A = B = -C = D = \frac{1}{2}. \qquad \text{(Equation 2.15)}$$

This allowed for the equations of motions to be developed. The values from Equation 2.15 were then implemented into their corresponding locations in Equation 2.8, and the exponentials were expanded into the sine and cosine equivalencies. The final forms of the equations of the equations of motion are thus

$$C_{10}(t) = \cos(g_0 t),$$
$$C_{01}(t) = -i\sin(g_0 t). \qquad \text{(Equation 2.18)}$$

An important detail to note is that the only case of interest for this system is when the excitation re-enters the field after the interaction time. This necessitates that

$$|C_{10}(T)| = |\cos(g_0 T)| = 1, \qquad \text{(Equation 2.19)}$$

for T being the interaction time, and that $g_0 T = n\pi$ for an integer n. This implies that the only possible phase induced upon a photon by the linear response (ϕ_0 from Equation 1.15) can be either 0 or π, else Equation 2.19 does not hold.

2.2 Single-Mode Two Photon Analysis

Next, the response of the TMD to two simultaneous single-frequency mode photons was determined. The thought experiment introduced in Section 2.1 is again considered, albeit with a two-photon state, a two-exciton state, and an intermediary state of one photon and one exciton. As a wave function the total state is written as

$$|\psi(t)\rangle \;=\; C_{20}(t)|20\rangle + C_{11}(t)|11\rangle + C_{02}(t)|02\rangle, \qquad \text{(Equation 2.20)}$$

where $|20\rangle$ represents the state of two existing photons and no excitons in the cavity, $|11\rangle$ is one photon and one exciton, and $|02\rangle$ corresponds to no photons and two excitons. The coefficient functions $C_{20}(t)$, $C_{11}(t)$, and $C_{02}(t)$ are the equations of motion of the respective states.

The objective for this part was to determine if the equation of motion of the pair of reflected photons could be made to experience a π-phase shift. For a qubit, the phase of the electric field of the photons must flip, i.e., if $C_{20}(t_0)$ is equal to one at the beginning of interaction, upon leaving the system it should be equal to negative one at time T. Due to the magnitude of the system necessarily being equivalent to one for a measurement, this phase shift requirement modifies Equation 2.19 to

$$|C_{20}(T) + 1| \approx 0. \qquad \text{(Equation 2.21)}$$

Since the phase shift of the linear response of the TMD, ϕ_0, must equal to 0 or π per Equation 2.19, it then follows from Equation 1.15 that the phase induced by the nonlinear response, ϕ_χ, must be some odd integer multiple of π. It is of tangential interest that if a TMD could be engineered to produce no phase shift in the linear response, then the auxiliary ϕ_0 phase shifters in Figure 1.3 could be removed from the gate.

Determining the impact of the relationships g_0 and χ upon ϕ_χ was the goal of the work presented in this chapter. Since these are in arbitrary units of energy, the energy steps presented by Planck's angular constant are absorbed into them like in Section 2.1. This system follows the same Hamiltonian in Equation 2.1, which when applied to Equation 2.20 via the Schrödinger Equation, develops to

$$\frac{\partial}{\partial t}|\psi(t)\rangle = -\frac{i}{\hbar} H(C_{20}(t)|20\rangle + C_{11}(t)|11\rangle + C_{02}(t)|02\rangle),$$

(Equation 2.22)

which the RHS was then expanded to

$$HC_{20}(t)|20\rangle = -i\sqrt{2}g_0 C_{20}(t)|11\rangle,$$
$$HC_{11}(t)|11\rangle = -i\sqrt{2}g_0(C_{11}(t)|20\rangle + C_{11}(t)|02\rangle),$$
$$HC_{02}(t)|02\rangle = -i\sqrt{2}g_0\left(C_{02}(t)|11\rangle + \sqrt{2}\frac{\chi}{g}C_{02}(\mathrm{t})|02\rangle\right), \quad \text{(Equation 2.23)}$$

with the LHS time derivatives of

$$\left|\dot{\psi}(t)\right\rangle = \dot{C}_{20}(t)|20\rangle + \dot{C}_{11}(t)|11\rangle + \dot{C}_{02}(t)|02\rangle. \quad \text{(Equation 2.24)}$$

Comparing coefficients of like states, this found the overall relationships to be

$$\dot{C}_{20}(t) = -i\sqrt{2}g_0 C_{11}(t),$$

$$\dot{C}_{11}(t) = -i\sqrt{2}g_0\big(C_{20}(t) + C_{02}(t)\big),$$

$$\dot{C}_{02}(t) = -i\sqrt{2}g_0\left(C_{11}(t) + \sqrt{2}\frac{\chi}{g_0}C_{02}(t)\right). \qquad \text{(Equation 2.25)}$$

Here, the rate of change of the two-photon state, $\dot{C}_{20}(t)$, depends solely upon the state equation of motion of the one photon and one exciton, which is expected as each photon begins to interact with the medium producing a state of one photon and one exciton until both photons are totally absorbed. The second equation is also intuitive, as the state of one exciton and one photon will fluctuate between either absolute state, depending on both. The two-exciton state is of particular interest, however, and depends upon the equation of one photon and one exciton, like the two-photon state, but has a self-dependency modulated by the ratio of the exciton interaction energy against the coupling constant, χ/g_0.

To find solutions for functions $C_{20}(t)$, $C_{11}(t)$, and $C_{02}(t)$, the Schrödinger Equation relations were first put into matrix notation as

$$\begin{pmatrix}\dot{C}_{20}(t)\\ \dot{C}_{11}(t)\\ \dot{C}_{02}(t)\end{pmatrix} = -i\sqrt{2}g_0\begin{pmatrix}0 & 1 & 0\\ 1 & 0 & 1\\ 0 & 1 & \sqrt{2}\frac{\chi}{g_0}\end{pmatrix}\begin{pmatrix}C_{20}(t)\\ C_{11}(t)\\ C_{02}(t)\end{pmatrix}. \qquad \text{(Equation 2.26)}$$

This has the characteristic equation

$$\lambda^3 + 2i\chi\lambda^2 + 4g_0^2\lambda + 4ig_0^2\chi = 0, \qquad \text{(Equation 2.27)}$$

with some general eigenvalue λ introduced via a three-by-three identity matrix. The solutions to this polynomial, λ_1, λ_2, and λ_3, can be found analytically, but are messy, and are left off the page. The equations of motion were then organized into a system of equations with general solution coefficients α_{ij} and the corresponding λ eigenvalues as

$$C_{20}(t) = \alpha_{11}\, e^{\lambda_1 t} + \alpha_{12}\, e^{\lambda_2 t} + \alpha_{13}\, e^{\lambda_3 t},$$
$$C_{11}(t) = \alpha_{21}\, e^{\lambda_1 t} + \alpha_{22}\, e^{\lambda_2 t} + \alpha_{23}\, e^{\lambda_3 t}\,,$$
$$C_{02}(t) = \alpha_{31}\, e^{\lambda_1 t} + \alpha_{32}\, e^{\lambda_2 t} + \alpha_{33}\, e^{\lambda_3 t}, \qquad \text{(Equation 2.28)}$$

with the time derivatives

$$\dot{C}_{20}(t) = \alpha_{11}\, \lambda_1 e^{\lambda_1 t} + \alpha_{12}\, \lambda_2 e^{\lambda_2 t} + \alpha_{13}\, \lambda_3 e^{\lambda_3 t},$$
$$\dot{C}_{11}(t) = \alpha_{21}\, \lambda_1 e^{\lambda_1 t} + \alpha_{22}\, \lambda_2 e^{\lambda_2 t} + \alpha_{23}\, \lambda_3\, e^{\lambda_3 t},$$
$$\dot{C}_{02}(t) = \alpha_{31} \lambda_1\, e^{\lambda_1 t} + \alpha_{32}\, \lambda_2 e^{\lambda_2 t} + \alpha_{33}\, \lambda_3\, e^{\lambda_3 t}\,. \qquad \text{(Equation 2.29)}$$

This system was then solved with an initial conditions boundary value. The first line in Equation 2.25 had the $C_{11}(t)$ in Equation 2.28 and $\dot{C}_{20}(t)$ in Equation 2.29 values plugged in:

$$\alpha_{11}\, \lambda_1 e^{\lambda_1 t} + \alpha_{12}\, \lambda_2 e^{\lambda_2 t} + \alpha_{13}\, \lambda_3 e^{\lambda_3 t} = -\, i\, \sqrt{2} g_0 \left(\alpha_{21}\, e^{\lambda_1 t} + \alpha_{22}\, e^{\lambda_2 t} + \alpha_{23}\, e^{\lambda_3 t} \right),$$

(Equation 2.30)

and the α_{2j} coefficients were then set in terms of the α_{1j} one, as

$$\alpha_{21} = \frac{i}{\sqrt{2}g_0}\lambda_1\alpha_{11},$$

$$\alpha_{22} = \frac{i}{\sqrt{2}g_0}\lambda_2\alpha_{12},$$

$$\alpha_{23} = \frac{i}{\sqrt{2}g_0}\lambda_3\alpha_{13}. \qquad \text{(Equation 2.31)}$$

This was also done with the third line in Equation 2.25, drawing from the corresponding $\dot{C}_{02}(t)$, $C_{11}(t)$, and $C_{02}(t)$ values in Equation 2.28 and Equation 2.29 to find

$$\alpha_{31}\lambda_1 e^{\lambda_1 t} + \alpha_{32}\lambda_2 e^{\lambda_2 t} + \alpha_{33}\lambda_3 e^{\lambda_3 t} =$$

$$-i\sqrt{2}g_0\left(\left(\alpha_{21}e^{\lambda_1 t} + \alpha_{22}e^{\lambda_2 t} + \alpha_{23}e^{\lambda_3 t}\right) + \sqrt{2}\frac{\chi}{g_0}\left(\alpha_{31}e^{\lambda_1 t} + \alpha_{32}e^{\lambda_2 t} + \alpha_{33}e^{\lambda_3 t}\right)\right).$$

(Equation 2.32)

This equation was separated by like terms and the α_{3j} coefficients were then written in terms of the α_{1j} variable,

$$\alpha_{31} = \frac{(\lambda_1)^2}{2i\frac{\chi}{g_0}+\lambda_1}\alpha_{11},$$

$$\alpha_{32} = \frac{(\lambda_2)^2}{2i\frac{\chi}{g_0}+\lambda_2}\alpha_{12},$$

$$\alpha_{33} = \frac{(\lambda_3)^2}{2i\frac{\chi}{g_0}+\lambda_3}\alpha_{13}, \qquad \text{(Equation 2.33)}$$

where the relationships from Equation 2.31 have been implemented. Then, Equation 2.28 was written solely in terms of α_{1j} coefficients and expressed as the matrix

$$\begin{pmatrix} C_{20}(t) \\ C_{11}(t) \\ C_{02}(t) \end{pmatrix} = \begin{pmatrix} 1 & 1 & 1 \\ i\frac{\lambda_1}{\sqrt{2}g_0} & i\frac{\lambda_2}{\sqrt{2}g_0} & i\frac{\lambda_3}{\sqrt{2}g_0} \\ \frac{\lambda_1^2}{2i\frac{\chi}{g_0}+\lambda_1} & \frac{\lambda_2^2}{2i\frac{\chi}{g_0}+\lambda_2} & \frac{\lambda_3^2}{2i\frac{\chi}{g_0}+\lambda_3} \end{pmatrix} \begin{pmatrix} \alpha_{11} \\ \alpha_{12} \\ \alpha_{13} \end{pmatrix}. \qquad \text{(Equation 2.34)}$$

The initial conditions were then introduced, defined at time $t = 0$ as

$$C_{20}(0) = 1,$$

$$C_{11}(0) = 0,$$

$$C_{02}(0) = 0. \qquad \text{(Equation 2.35)}$$

Then, the matrix of coefficients in Equation 2.31 was inverted against these values from the left,

$$\begin{pmatrix} 1 & 1 & 1 \\ i\frac{\lambda_1}{\sqrt{2}g_0} & i\frac{\lambda_2}{\sqrt{2}g_0} & i\frac{\lambda_3}{\sqrt{2}g_0} \\ \frac{\lambda_1^2}{2i\frac{\chi}{g_0}+\lambda_1} & \frac{\lambda_2^2}{2i\frac{\chi}{g_0}+\lambda_2} & \frac{\lambda_3^2}{2i\frac{\chi}{g_0}+\lambda_3} \end{pmatrix}^{-1} \begin{pmatrix} 1 \\ 0 \\ 0 \end{pmatrix} = \begin{pmatrix} \alpha_{11} \\ \alpha_{12} \\ \alpha_{13} \end{pmatrix}, \qquad \text{(Equation 2.36)}$$

leading to the α_{1j} coefficients in terms of the eigenvalues, found as

$$\alpha_{11} = \frac{\lambda_2\lambda_3\,(-ig_0\lambda_1+2\chi)}{2i(\lambda_1-\lambda_2)(\lambda_1-\lambda_3)\chi},$$

$$\alpha_{12} = \frac{\lambda_1\lambda_3\,(-ig_0\lambda_2+2\chi)}{2(\lambda_2-\lambda_1)(\lambda_2-\lambda_3)\chi},$$

$$\alpha_{13} = \frac{\lambda_1\lambda_2\,(-ig_0\lambda_3+2\chi)}{2(\lambda_3-\lambda_1)(\lambda_3-\lambda_2)\chi}. \qquad \text{(Equation 2.37)}$$

$C_{20}(t)$ can then be written completely in terms of these eigenvalues, and was written as

$$C_{20}(t) = \left(\frac{\lambda_2\lambda_3\,(-ig_0\lambda_1+2\chi)}{2i(\lambda_1-\lambda_2)(\lambda_1-\lambda_3)\chi}\right)e^{\lambda_1 t} + \left(\frac{\lambda_1\lambda_3\,(-ig_0\lambda_2+2\chi)}{2(\lambda_2-\lambda_1)(\lambda_2-\lambda_3)\chi}\right)e^{\lambda_2 t} + \left(\frac{\lambda_1\lambda_2\,(-ig_0\lambda_3+2\chi)}{2(\lambda_3-\lambda_1)(\lambda_3-\lambda_2)\chi}\right)e^{\lambda_3 t}$$

(Equation 2.38)

At time T, it was established with Equation 2.21 that the amplitude of $C_{20}(T)$ should be approximately negative one or approach it. It was also required in Section 2.1 that the time periods for a useful phase shift are a factor of $g_0T = n\pi$, for some integer π. Therefore, the case of $|C_{20}(T)+1| \rightarrow 0$ as a function of the ratio χ/g_0 is of interest, as this determines the state of the returned photons as a function of the TMD's nonlinearity.

Figure 2.1 shows a plot of $|C_{20}(T)+1|$, where for the sake of simplicity g_0 is restricted to a value of one, thus $\chi/g_0 = \chi$ and $g_0T = T$. The goal of this plotting is to specify parameter restrictions so that at the end of interaction, at time T, the complex electric field E_{refl} has a π-rad phase shift relative to E_c. It is interesting that the integer multiples of πT do not necessarily correlate with their own integers multiples, for example in Figure 2.1 a.) it is seen that both 3π

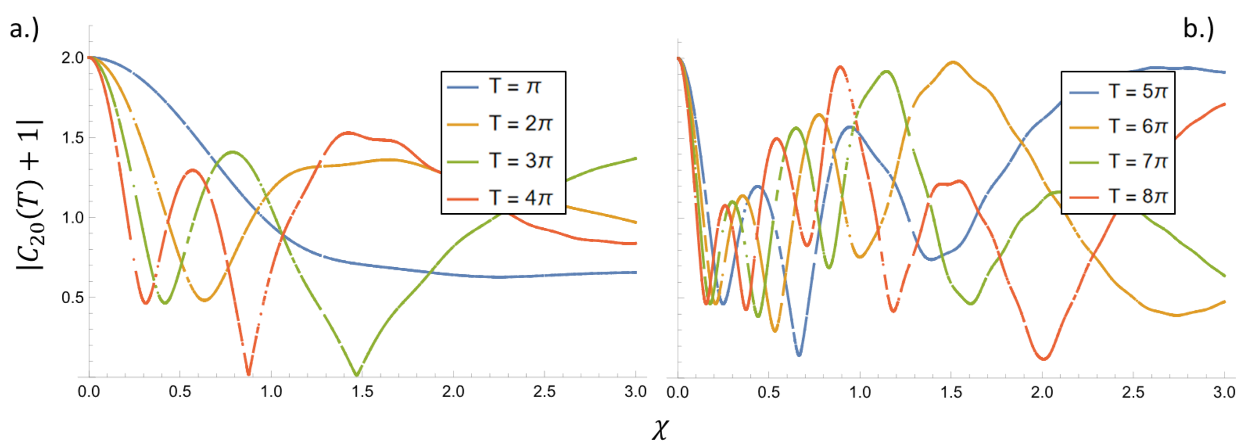

Figure 2.1 Two-Photon state vs. variable nonlinearity

and 4π can exhibit a close approach to $C_{20}(T) = 0$, as desired, but the higher integer-multiples of these, 6π and 8π, do not get as close. It is also of interest of that dependency upon χ has oscillating sweet spots and that if it is too weak or too strong it disrupts the ability of the photons to receive the intended phase shift.

Chapter 3: The Multimode Case

3.1 Cavity Properties

This chapter generalizes the single-mode results found in Chapter 2 to a more realistic multimode analysis, and then extends the analysis to include a perfectly reflecting barrier in the two-photon case. The goal was to assess the impact of the system's nonlinear response on the phase of the outgoing, reflected photons. Primarily, the concern was if only small changes in the χ of the TMD could produce a flip in the total phase of the photons.

By considering the monolayer TMD as a plane of atomic dipoles, a single photon was again analyzed first. Placing an atomically thin TMD parallel to a perfect reflector (reflection coefficient $r = -1$), positioned away at some distance d, constructs the desired cavity, as portrayed in Figure 3.1. A single photon, opposite the reflector, enters the cavity orthogonal to the plane of the TMD. The one-dimensional electric field components were described as

$$E_c(z,t) = Ee^{-i\omega t+ikz,}$$

$$E_{refl}(z,t) = E_{refl}e^{-i\omega t-ikz},$$

$$E_R(z,t) = E_Re^{-i\omega t+ikz},$$

$$E_L(z,t) = E_Le^{-i\omega t-ikz}. \quad \text{(Equation 3.1)}$$

Here, E_c represents the magnitude of the applied electric field from the incident photon, E_{refl} is the magnitude of the reflected electric field, E_R is the magnitude of the electric field traveling in the positive z direction in the space $0 < z < d$, and, similarly, E_L is the magnitude of the electric field traveling in the negative z direction in the space $z < 0$. Lastly, $k = \omega/c$, with ω the angular frequency of the incident light and c is the speed of light.

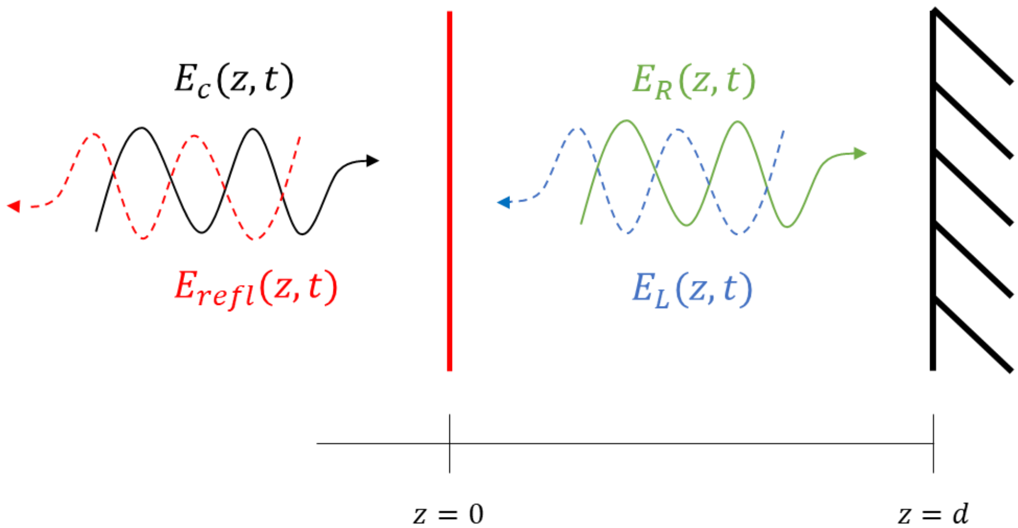

Figure 3.1 Proposed Optical Cavity

In real space the total electric field of the TMD, at general position $\boldsymbol{r}$, is the sum of the driving electric field from the cavity excitation and all the radiated fields from each atomic component. If each atom is regarded as an individual dipole moment then the total electric field appears as

$$\boldsymbol{E}(\boldsymbol{r}) = \boldsymbol{E}_c(\boldsymbol{r}) + \sum_{i=1}^{N} \boldsymbol{E}_i(\boldsymbol{r}), \qquad \text{(Equation 3.2)}$$

for $\boldsymbol{E}(\boldsymbol{r})$ is the net local electric field at the position of the TMD, $\boldsymbol{E}_c(\boldsymbol{r})$ is the electric field of the incident photon, and $\boldsymbol{E}_i(\boldsymbol{r})$ is the field of each dipole in the array.

The scattered field from an individual dipole is given by

$$\boldsymbol{E}_i(\boldsymbol{r}) = G_a(\boldsymbol{Z}_i)d_i, \qquad \text{(Equation 3.3)}$$

where $G_a(\boldsymbol{Z}_i)$ is the general dipole propagation tensor for position coordinates $\boldsymbol{Z}_i = \boldsymbol{z} - \boldsymbol{z}_i$ and d_i is the total local electric field for each dipole. This local electric field is a function of each dipole's polarizability, $\alpha(\omega')$, and is given as

$$d_i = \alpha(\omega')\boldsymbol{E}(\boldsymbol{z}_i), \qquad \text{(Equation 3.4)}$$

with $\omega' = \omega - \omega_a$ as the detuning frequency between the driving photon and the individual dipole frequency (assumed constant across all dipoles). The photon's frequency is $\omega = 2\pi c/\lambda$, for c is the speed of light and λ is its wavelength while the dipole transition frequency is $\omega_a = 2\pi c/\lambda_a$, where λ_a is the dipole's transition wavelength. The polarizability, $\alpha(\omega')$, is generally a tensor but was taken one-dimensionally under the assumption the light is a plane wave perfectly orthogonally upon each dipole.

The linear polarizability of each dipole contributes individually as a summation to the overall polarizability of the lattice. Through an adjusted Bloch theorem treatment, as considered in Shahmoon *et al* (34), the ensemble was limited to a two-dimensional planar crystal, with each dipole's polarizability assumed to contribute to the dielectric response of the entire array in a cooperative resonance. The application of a two-dimensional scattering matrix results in an effective scalar polarizability of the whole TMD of

$$\alpha_e = -\frac{3}{4\pi^2}\epsilon_0\lambda_0^2\frac{\gamma/2}{\omega' - \Delta + i(\gamma+\Gamma)/2}, \qquad \text{(Equation 3.5)}$$

for ϵ_0 is the permittivity of free space and γ is the radiative decay rate of the dipoles. The corresponding reflection scattering amplitude is then equivalent to

$$r = -\frac{i(\gamma+\Gamma)/2}{\omega'-\Delta+i(\gamma+\Gamma)/2}, \qquad \text{(Equation 3.6)}$$

while the transmission amplitude is

$$\tau = -\frac{\omega'-\Delta}{\omega'-\Delta+i(\gamma+\Gamma)/2}. \qquad \text{(Equation 3.7)}$$

For the cooperative resonance, Δ, is the detuning between it and the incident light and Γ is its radiative decay rate. This decay is found to be

$$\Gamma = \gamma\frac{3}{4\pi}\left(\frac{\lambda}{a}\right)^2 - \gamma, \qquad \text{(Equation 3.8)}$$

with lattice constant *a* and nonradiative losses neglected. The resonance detuning, Δ, follows as

$$\Delta = \frac{i}{2}\Gamma - \frac{3}{2}\gamma\lambda\sum_{n\neq 0} G(0, z_n), \qquad \text{(Equation 3.9)}$$

where $G(0, \mathrm{z}_n)$ is the transverse portion of the general Green's function satisfying the electromagnetic wave equation and z_n is the spatial position of the *n*th dipole from center.

With these scattering coefficients, the magnitudes of the electric field equations can be re-examined. Just inside the TMD, in the space approaching *z* from the right (the $z = 0^+$ neighborhood), the rightward traveling electric field, E_R, is the sum of the transmission component of the initial pulse magnitude, E_c, and the component of the leftward field, E_L, returned from the mirror. Inversely, the field just outside the TMD, in the space approaching the

TMD from the left (the $z = 0^-$ neighborhood), the total outwardly-leaving electric field of the system, E_{refl}, is the combined reflected portion of the driving E_c field and the transmitted portion of the leftward traveling field, E_L. These are, respectively,

$$E_R = \tau E_c + r E_L,$$
$$E_{refl} = r E_c + \tau E_L. \qquad \text{(Equation 3.10)}$$

At $z = d$, Equation 3.1 was used to find

$$E_R(d,t) = E_R e^{-i\omega t - i\phi}\ ,$$
$$E_L(d,t) = E_L e^{-i\omega t + i\phi}, \qquad \text{(Equation 3.11)}$$

with $\phi = 2n\pi - kd$, for n an integer. In this chapter, the use of the variable ϕ expressly indicates the phase shift operator of the photons gained over the course of traveling across d and back and is not the same as the phase of the overall qubit discussed in Chapter 1. The relative phase of the qubit is considered as the classical phase of an electric field and is the real argument of the complex field. Assuming perfect reflection at $z = d$, Equation 3.11 was developed to

$$E_R e^{-i\phi} = -E_L e^{i\phi},$$
$$E_R = -E_L e^{2i\phi}, \qquad \text{(Equation 3.12)}$$

which was plugged into Equation 3.10 to find

$$E_R = \frac{\tau}{1+e^{-2i\phi}r} E_c$$

$$E_L = -\frac{\tau}{r+e^{2i\phi}} E_c$$

$$E_{refl} = \left(r - \frac{\tau^2}{r+e^{2i\phi}}\right) E_c \qquad \text{(Equation 3.13)}$$

The specific cavity design was inspired by recent work by Wild *et al* (23) and Zhou *et al* (35), which takes advantage of the potential for a high reflectivity of the TMD. The cavity presented in this thesis differs in that the reflector opposite the TMD is considered perfect rather than having some finite transmission rate. In both cases, however, the goal was to increase interaction between a single photon and the TMD, and in this way increase the effect of the nonlinearity. Tuning the cavity to a resonance, where the sum of the traveling phase shift 2ϕ and the phase shifts acquired upon the reflection equals an integer multiple of 2π, will achieve this nonlinearity increase. This condition is equivalent to maximizing the field at the TMD, which is calculated by adding E_R and E_L, as given by Equation 3.13. This can be achieved by tuning either the cavity length (and hence 2ϕ) or the incident light frequency of ω (and hence ω') (23,34–36).

Because of the cavity design, regardless of resonance or not, all the incident light is always reflected. Ideally, the reflected field will experience a phase change that is different depending upon whether there are one or two incident photons. The two-photon case was predicted to generate two excitons who, through their interaction energy χ, will modify the system's resonant frequency and change the phase of the reflected field (37,38).

Figure 3.2 demonstrates that the real argument of E_{refl} can indeed undergo a rapid phase flip for only small shifts in ϕ and ω'. Figure 3.2 a.) shows the phase of E_{refl} flipping as a function of the detuning with the photon's angular phase shift kept constant at ϕ = 6.3, near 2π, and Figure 3.2 b.) also shows the phase flipping but with E_{refl} as a function of the photon's angular phase while the frequency detuning is kept small, at ω' = 0.03. This figure is to show that it is simply possible to elicit a total phase flip of the complex electric field for only small changes in the system parameters.

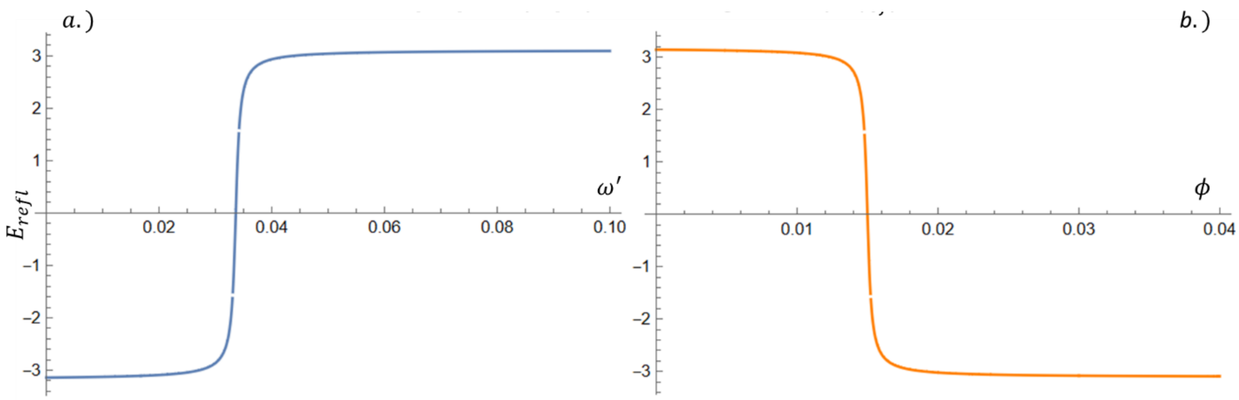

Figure 3.2 Rapid phase flip of the real argument of E_{refl}

3.2 Annihilation Operator Equations of Motion

In this section a quantum mechanical description of a multimode single-photon wavepacket in within the cavity is described. When performing the original derivation, the aim was to find a self-consistent equation of motion for the annihilation operator the photon mode of the polariton. To do this, firstly the equation of motion of the annihilation operator of the exciton needed to be found, due to the photon creation operator's dependency upon it. This photon operator was then

to be analyzed against the detuning frequency between the photons and the dipoles, ω', the relative phase shift operators of the photon across the resonator, ϕ, and the exciton self-resonance energy χ. The field at the TMD is given by sum of $E_R(0,t)$ and $E_L(0,t)$. With Equation 3.6, Equation 3.7, and Equation 3.13; this was found to be

$$E_{TMD} = \frac{2\omega'(1-e^{2i\phi})}{i\gamma(1-e^{2i\phi})-2\omega' e^{2i\phi}} E_c. \qquad \text{(Equation 3.14)}$$

The equations were derived in the Heisenberg picture, whereby the photon-exciton system was treated as a quantum mechanical harmonic oscillator with corresponding creation and annihilation operators. The Hamiltonian is

$$H = \int_{-\infty}^{\infty} \left(g(\omega') a_\omega(t) e^{-i\omega' t} b^\dagger(t) + g^\star(\omega') a_\omega^\dagger(t) e^{i\omega' t} b \right) d\omega + \chi\, b^\dagger(t) b^\dagger(t) b(t) b(t),$$

(Equation 3.15)

where $a_\omega(t)$, $a_\omega^\dagger(t)$, $b(t)$, and $b^\dagger(t)$ are the equations of motion for annihilation of a photon, creation of a photon, annihilation of an exciton, and creation of an exciton, respectively. Each operator is a function of time, and the photon operators are also functions of the frequency of the incident photon, ω, but this dependency is put as a subscript. Here the factor $g(\omega')$ is found as

$$g(\omega') = g_0 \left(\frac{2\omega'(1-e^{2i\phi})}{i\gamma(1-e^{2i\phi})-2\omega' e^{2i\phi}} \right), \qquad \text{(Equation 3.16)}$$

where g_0 is the photon-exciton coupling constant used in Chapter 2. If the exciton decay is purely radiative, then $g_0^2 = \gamma/2$, and the parenthetical is the proportionality factor between the field in the cavity and the incident field, as seen in Equation 3.14.

The overall state of the single-photon system can be written as

$$|\psi\rangle = \int_{-\infty}^{\infty} C_{10}(\omega, t) a_\omega^\dagger(t) d\omega' |00\rangle + C_{01}(t)|01\rangle, \qquad \text{(Equation 3.17)}$$

with $|00\rangle$ representing the photon vacuum state and exciton vacuum state and $|01\rangle$ as the photon vacuum state and the exciton excited field state. The $C_{10}(\omega, t)$ equation of motion governs the behavior of the photon and the $C_{01}(t)$ is the equation of motion for the exciton.

To address the two-photon case, within Heisenberg picture was used, the derived equation of motion operators become:

$$\dot{b}(t) = -\frac{i}{\hbar}[b(t), H]$$

$$\dot{a}_\omega(t) = -\frac{i}{\hbar}[a_\omega(t), H]$$

$$\dot{b}^\dagger(t) = -\frac{i}{\hbar}[b^\dagger(t), H]$$

$$\dot{a}_\omega^\dagger(t) = -\frac{i}{\hbar}[a_\omega^\dagger(t), H], \qquad \text{(Equation 3.18)}$$

which, when the commutators are applied, gave the equations

$$\dot{b}(t) = -\frac{i}{\hbar}\int_{-\infty}^{\infty} g(\omega')\, a_\omega(t) e^{-i\omega' t} d\omega' - 2\frac{i}{\hbar}\chi\, b^\dagger(t) b(t) b(t)$$

$$\dot{a}_\omega(t) = -\frac{i}{\hbar} g^\star(\omega') b(t) e^{i\omega' t}$$

$$\dot{b^\dagger}(t) = \frac{i}{\hbar}\int_{-\infty}^{\infty} g(\omega')\, a_\omega(t) e^{i\omega' t} d\omega + 2\frac{i}{\hbar}\chi\, b^\dagger(t) b(t) b(t)$$

$$\dot{a^\dagger}_\omega(t) = \frac{i}{\hbar} g^\star(\omega') b(t) e^{-i\omega' t}. \qquad \text{(Equation 3.19)}$$

From here forward, like in Section 2.1, the quantities of $\hbar$ were rolled into the corresponding χ and g_0 values.

The formal integration of $\dot{a}_\omega(t)$ in Equation 3.19 was taken for time by introducing the dummy integration variable t'. The photon annihilation operator $a_\omega(t)$ was then found as

$$a_\omega(t) - a_\omega(0) = -\frac{i}{\hbar}\int_0^t g^\star(\omega')e^{i\omega' t'} b(t')dt', \qquad \text{(Equation 3.20)}$$

where $a_\omega(0)$ is the constant initial value of $a_0(t)$ for $t = 0$.

This was substituted into the equation for $\dot{b}(t)$ in Equation 3.19 and rearranged, finding

$$\dot{b}(t) = -i\int_{-\infty}^{\infty} g\,(\omega')\left(-i\int_0^t g^\star(\omega')e^{i\omega' t'} b(t')dt' + a_\omega(0)\right)e^{-i\omega' t}d\omega' - 2i\chi b^\dagger(t)b(t)b(t)$$

$$= -\int_0^t b(t')\int_{-\infty}^{\infty} |\,g(\omega')|^2 e^{-i\omega'(t-t')}d\omega' dt' - i\int_{-\infty}^{\infty} g(\omega')\,a_\omega(0)e^{-i\omega' t}d\omega' -$$

$$2i\chi b^\dagger(t)b(t)b(t). \qquad \text{(Equation 3.21)}$$

For notation, the second component of Equation 3.21 was replaced with $h(t)$ such that

$$h(t) = -i\int_{-\infty}^{\infty} g(\omega')\,a_\omega(0)e^{-i\omega' t}d\omega'. \qquad \text{(Equation 3.22)}$$

Through algebraic reductions, $|g(\omega')|^2$ was found as

$$|g(\omega')|^2 = 4g_0^2\sin^2\phi\left(1 + \frac{1}{2}\frac{i\gamma e^{-2i\phi}}{\omega' - \gamma\sin\phi e^{-i\phi}} - \frac{1}{2}\frac{i\gamma e^{-2i\phi}}{\omega' - \gamma\sin(\phi)e^{i\phi}}\right), \qquad \text{(Equation 3.23)}$$

and then Equation 3.22 and Equation 3.23 were both substituted into Equation 3.20 to give

$$\dot{b}(t) = h(t) + 4g_0^2 \sin^2\phi \int_0^t b(t') \left(\int_{-\infty}^{\infty} e^{-i\omega'(t-t')} \left(1 + \frac{1}{2} \frac{i\gamma e^{-2i\phi}}{\omega' - \gamma \sin\phi e^{-i\phi}} - \frac{1}{2} \frac{i\gamma e^{-2i\phi}}{\omega' - \gamma \sin(\phi) e^{i\phi}} \right) d\omega' \right) dt' - 2i\chi b^\dagger(t) b(t) b(t). \quad \text{(Equation 3.24)}$$

To further reduce this, the double integral inside $\dot{b}(t)$ in Equation 3.24 was evaluated. Through calculus of residuals, Fourier transform treatments, and algebraic manipulations the integral over *dω'* was transformed to

$$-4g_0^2 \sin^2(\phi) \int_0^t b(t') \left(\int_{-\infty}^{\infty} e^{-i\omega(t-t')} \left(1 + \frac{1}{2} \frac{i\gamma e^{-2i\phi}}{\omega - \gamma \sin\phi e^{-i\phi}} - \frac{1}{2} \frac{i\gamma e^{-2i\phi}}{\omega - \gamma \sin(\phi) e^{i\phi}} \right) d\omega \right) dt'$$
$$= -4g_0^2 \sin^2(\phi) \left(\pi b(t) + \pi\gamma e^{-2i\phi} \int_0^t b(t')\, e^{-i\gamma \sin(\phi) e^{-i\phi}(t-t')} dt' \right).$$

(Equation 3.25)

The shorthand variables η and p were introduced such that

$$\eta = 4\pi g_0^2 \quad \text{(Equation 3.26)}$$

and

$$p = \sin(\phi)\, e^{-i\phi}. \quad \text{(Equation 3.27)}$$

Equation 3.25 was shortened and substituted into Equation 3.24 for a more compact form of $\dot{b}(t)$:

$$\dot{b}(t) = h(t) - \eta \sin^2(\phi)\, b(t) - \eta\gamma p^2 \int_0^t b(t')\, e^{-i\gamma p(t-t')} dt' - i\chi b^\dagger(t) b(t) b(t).$$

(Equation 3.28)

In the two-photon case, the final term in Equation 3.28 was found to be difficult to treat exactly. Instead, the constant β was defined as the approximate expectation value of two excitons existing simultaneously. Since the interaction energy χ is inherently the near-field and Coulombic interactions between two separate excitons, the expectation value approximation is justified by determining the likelihood of χ being involved in any given interaction between two photons and the TMD. The expectation was written as

$$\beta = \langle b^\dagger(t) b(t) \rangle, \qquad \text{(Equation 3.29)}$$

and then used to give the scalar coefficient

$$b^\dagger(t) b(t) b(t) \approx \left\langle b^\dagger(t) b(t) \right\rangle b(t) = \beta b(t). \qquad \text{(Equation 3.30)}$$

This was then used to further simplify Equation 3.28 to

$$\dot{b}(t) = h(t) - (\eta \sin^2(\phi) + i\chi\beta) b(t) - \eta\gamma p^2 \int_0^t b(t')\, e^{-i\gamma p(t-t')} dt'.$$

(Equation 3.31)

with the assumption that $\beta = 0$ in the single-photon case. The variable χ' was then introduced:

$$\chi' = \eta \sin^2(\phi) + i\chi\beta. \qquad \text{(Equation 3.32)}$$

Next, the time derivative of Equation 3.31 was taken, giving

$$\ddot{b}(t) = \dot{h}(t) - \chi'\dot{b}(t) - \eta\gamma p^2 \left(\frac{d}{dt}\int_0^t b(t')\, e^{-i\gamma p(t-t')}dt'\right)$$

$$= \dot{h}(t) - \chi'\dot{b}(t) - \eta\gamma p^2 \left(-i\gamma p \int_0^t b(t')\, e^{-i\gamma p(t-t')}dt' + b(t)\right)$$

$$= \dot{h}(t) - \eta\gamma p^2 b(t) - \chi'\dot{b}(t) + i\eta\gamma^2 p^3 \int_0^t b(t')\, e^{-i\gamma p(t-t')}dt'.$$

(Equation 3.33)

The integral across dt' in Equation 3.33 is also present in Equation 3.31, which was rearranged to give the equivalency

$$\int_0^t b(t')\, e^{-i\gamma p(t-t')}dt' = -\frac{1}{\eta\gamma p^2}\left(-h(t) + \chi' b(t) + \dot{b}(t)\right). \quad \text{(Equation 3.34)}$$

Substituting this back into Equation 3.32 produced

$$\ddot{b}(t) = i\gamma p h(t) + \dot{h}(t) - (\eta\gamma p^2 + i\gamma p\chi')b(t) - (i\gamma p + \chi')\dot{b}(t).$$

(Equation 3.35)

Then, the solution to the homogeneous case of $\ddot{b}(t)$, i.e., when $h(t) = \dot{h}(t) = 0$, was considered. The general solution for this case is

$$b(t) = e^{\lambda t} b(0), \quad \text{(Equation 3.36)}$$

for $b(0)$ is the initial condition, $t = 0$. The following time derivatives are

$$\dot{b}(t) = \lambda e^{\lambda t} b(0) \qquad \text{(Equation 3.37)}$$

and

$$\ddot{b}(t) = \lambda^2 e^{\lambda t} b(0). \qquad \text{(Equation 3.38)}$$

To find the eigenvalues λ, the RHS of Equation 3.38 was set equal to the RHS of Equation 3.35, noting that $h(t) = \dot{h}(t) = 0$. Then Equation 3.36 and Equation 3.37 were plugged into their respective instances of $b(t)$ and $\dot{b}(t)$ in Equation 3.35, producing

$$\lambda^2 e^{\lambda t} b(0) = -(\eta\gamma p^2 + i\gamma p\chi')e^{\lambda t} b(0) - (i\gamma p + \chi')\lambda e^{\lambda t} b(0).$$

(Equation 3.39)

Equation 3.39 was then reduced and rearranged to find the quadratic for *t* = *0* of

$$\lambda^2 + (i\gamma p + \chi')\lambda + (\eta\gamma p^2 + i\gamma p\chi') = 0, \qquad \text{(Equation 3.40)}$$

with the eigenvalues

$$\lambda_1 = \frac{-(i\gamma p+\chi') + \sqrt{(i\gamma p+\chi')^2 - 4(\eta\gamma p^2 + i\gamma p\chi')}}{2},$$

$$\lambda_2 = \frac{-(i\gamma p+\chi') - \sqrt{(i\gamma p+\chi')^2 - 4(\eta\gamma p^2 + i\gamma p\chi')}}{2}. \qquad \text{(Equation 3.41)}$$

These were then used to build the integrating factors for the inhomogeneous case of Equation 3.35. In the case $h(t) \neq 0$ and $\dot{h}(t) \neq 0$, the solutions were assumed to be of the form

$$b(t) = A_1 \left(e^{\lambda_1 t} b(0) + e^{\lambda_1 t} \int_0^t e^{-\lambda_1 t'} \, h(t') dt' \right) + A_2 \left(e^{\lambda_2 t} b(0) + e^{\lambda_2 t} \int_0^t e^{-\lambda_2 t'} \, h(t') dt' \right),$$

(Equation 3.42)

with the shorthand notation equations

$$b_1(t) = e^{\lambda_1 t} b(0) + e^{\lambda_1 t} \int_0^t e^{-\lambda_1 t'} \, h(t') dt',$$

$$b_2(t) = e^{\lambda_2 t} b(0) + e^{\lambda_2 t} \int_0^t e^{-\lambda_2 t'} \, h(t') dt',$$

(Equation 3.43)

and their time derivatives

$$\dot{b}_1(t) = h(t) + \lambda_1 e^{\lambda_1 t} b(0) + \lambda_1 \int_0^t e^{-\lambda_1 (t-t')} \, h(t') dt'$$

$$= h(t) + \lambda_1 b_1(t),$$

$$\dot{b}_2(t) = h(t) + \lambda_2 e^{\lambda_2 t} b(0) + \lambda_2 \int_0^t e^{-\lambda_2 (t-t')} \, h(t') dt'$$

$$= h(t) + \lambda_2 b_2(t).$$

(Equation 3.44)

Through the values for $\dot{b}_1(t)$ and $\dot{b}_2(t)$ in Equation 3.44, $\dot{b}(t)$ was derived from Equation 3.42 to be

$$\dot{b}(t) = A_1 \dot{b}_1(t) + A_2 \dot{b}_2(t)$$

$$= A_1 \big(h(t) + \lambda_1 b_1(t) \big) + A_2 \big(h(t) + \lambda_2 b_2(t) \big).$$

(Equation 3.45)

Setting Equation 3.45 equal to Equation 3.31, and comparing coefficients of the like terms $h(t)$, it was found that

$$A_1 + A_2 = 1. \qquad \text{(Equation 3.46)}$$

Furthermore, the time derivative of Equation 3.45 was taken, and then the forms of $\dot{b}_1(t)$ and $\dot{b}_2(t)$ from Equation 3.44 were plugged in, producing

$$\ddot{b}(t) = A_1\left(\dot{h}(t) + \lambda_1 \dot{b}_1(t)\right) + A_2\left(\dot{h}(t) + \lambda_2 \dot{b}_2(t)\right)$$

$$= A_1\left(\dot{h}(t) + \lambda_1 h(t) + \lambda_1^2 b_1(t)\right) + A_2\left(\dot{h}(t) + \lambda_2 h(t) + \lambda_2^2 b_2(t)\right).$$

(Equation 3.47)

Equation 3.35 was then set equal to Equation 3.47, which gave

$$i\gamma p h(t) + \dot{h}(t) - (\eta\gamma p^2 + i\gamma p\chi')b(t) - (i\gamma p + \chi')\left(A_1\big(h(t) + \lambda_1 b_1(t)\big) + A_2\big(h(t) + \lambda_2 b_2(t)\big)\right) = A_1\left(\lambda_1 h(t) + \lambda_1^2 \dot{b}_1(t)\right) + A_2\left(\lambda_2 h(t) + \lambda_2^2 \dot{b}_2(t)\right), \qquad \text{(Equation 3.48)}$$

where, again, only coefficients of the like terms $h(t)$ were compared. Through use Equation 3.43, Equation 3.44, and Equation 3.45, the eigenvalues and inhomogeneous solution coefficients were found to have the relationship

$$\lambda_1 A_1 + \lambda_2 A_2 = -\chi'. \qquad \text{(Equation 3.49)}$$

With Equation 3.46 and Equation 3.49, the general solution coefficients were then found as

$$A_1 = \frac{\chi' + \lambda_2}{\lambda_2 - \lambda_1}$$

$$A_2 = \frac{\chi' + \lambda_1}{\lambda_1 - \lambda_2}. \qquad \text{(Equation 3.50)}$$

The equation $b(t)$, as formulated in Eq. 3.42, was rewritten with these coefficients as

$$b(t) = \sum_{j=1,2} A_i \left(e^{\lambda_j t} b(0) + \int_0^t e^{\lambda_j (t-t')} h(t) dt' \right). \qquad \text{(Equation 3.51)}$$

Lastly, Equation 3.22 was substituted back in for $h(t)$, along with a Fourier transformation to the time-integration component, resulting in the general equation of motion for the full exciton annihilation operator

$$b(t) = \sum_{j=1,2} A_j \left(e^{\lambda_j t} b(0) - i \int_{-\infty}^{\infty} g(\omega') \frac{a_\omega(0)}{\lambda_j + i\omega'} e^{-i\omega' t} d\omega' \right). \qquad \text{(Equation 3.52)}$$

Thus, an equation of motion of the exciton annihilation operator was found that could be substituted into Equation 3.20 to find the photon annihilation operator as a function of time.

3.3 Estimating the Reflected Field Phase Shift in the Two-Photon Case

The two-photon case is difficult to solve analytically. As such, the constant β was introduced under the assumption the two-photon case is identical to the single-photon case except for the for the presence of the $\chi\beta$ term in Equation 3.30. With that equation solved with the nonlinear $\chi\beta$ component, the question was whether a small change in the nonlinear response can induce a phase flip in the field leaving the cavity, E_{refl}, on the order of the in-principle phase changes demonstrated in Figure 3.2. In this section the phase shift induced by χ_β was determined and qualitatively compared between variations in the parameters ϕ, ω', and γ.

The spectrum of the incident electric field, E_c, in the single photon case, is given by

$$f_0(\omega) = \langle 00|a_\omega(t)|10\rangle, \qquad \text{(Equation 3.53)}$$

while the spectrum of the reflected field after the interaction (as $t \rightarrow \infty$) is, via Equation 3.13,

$$f_{refl}(\omega) = \left(r - \frac{\tau^2}{r + e^{2i\phi}}\right)\langle 00|a_\omega(t \ \rightarrow \ \infty)|10\rangle. \qquad \text{(Equation 3.54)}$$

The photon annihilation operator equation of motion $a_\omega(t)$ was applied from Equation 3.19, with the $b(t)$ component integrated from Equation 3.51, and the state vector $|00\rangle$ assuming the vacuum state and $|10\rangle$ as the initial state of one photon and no exciton. If the spectrum of the incident field is defined as the function $f_0(\omega)$ and the spectrum of the outgoing field (i.e., E_{refl}) of the oscillator is the function $f_{refl}(\omega)$, then Equation 3.54 can be expanded to

$$f_{refl}(\omega) = \left(r - \frac{\tau^2}{e^{2i\phi} + r}\right)\left(1 - 2\pi|g(\omega)|^2 \sum_j \frac{A_j}{\lambda_j + i\omega'}\, d\omega\right) f_0(\omega).$$

(Equation 3.53)

The second parenthetical term here has the only dependency on the nonlinear response χ implicitly through the eigenvalues λ_j and the inhomogeneous equation solution coefficients A_j. Here the expectation value approximation β was merged into the subscript of χ, such that

$$\chi_\beta = \chi * \beta. \qquad \text{(Equation 3.54)}$$

The values for A_j from Equation 3.50 were then plugged in, and the placeholder variables of η, p, and χ' are replaced with their original values. The second parenthetical expands as a function of the approximate nonlinear response; the function, $\Phi(\chi_\beta)$, becomes

$$\Phi(\chi_\beta) = 1 + 2\pi|g(\omega)|^2 \left((\omega - \chi)i - 2\pi\gamma \sin^2\phi \, (1 - \frac{ie^{-2i\phi}}{e^{-i\phi}\sin\phi - \frac{\omega}{\gamma}}\right)^{-1}.$$

(Equation 3.55)

Note here the absence of the coupling constant g_0, which has been set to $g_0^2 = \gamma/2$ for no nonradiative losses.

The resulting total value of Φ relies on the frequency detuning ω' (and its relation to the radiative rate of the excitons), the phase shift of the photons across the resonator ϕ, the dipoles' coupling constant g_0, and the nonlinear response χ_β. As ϕ and ω' each shrink, and possibly while g_0 grows, the phase flip was expected to become more rapid across small changes of χ_β. This was investigated primarily to determine the how fast the speed, per se, changes in χ_β such that the output value of Φ could have an entire sign flip, i.e., a phase flip.

For some arbitrary example values, the real component of Φ was modeled as a function of χ_β in Figure 3.3 for constants γ = 0.1 and ω' = 0.01 for various values of ϕ. The physical units of these values are temporarily ignored to instead investigate the orders of magnitude impact each one has upon Φ as a function of χ_β. Figure 3.3 a.) and b.) demonstrates strongly how important round-trip resonance is to the strength of the nonlinear effect; when ϕ approaches 2π as in Figure 3.3 b.) the phase of Φ flips very rapidly against only small changes in χ_β, but when ϕ = 6.35, or only 0.07 radians off an integer multiple of π, the phase occurs much slower.

It was guessed that the shift in the phase operator ϕ would follow a cyclic patter, with the

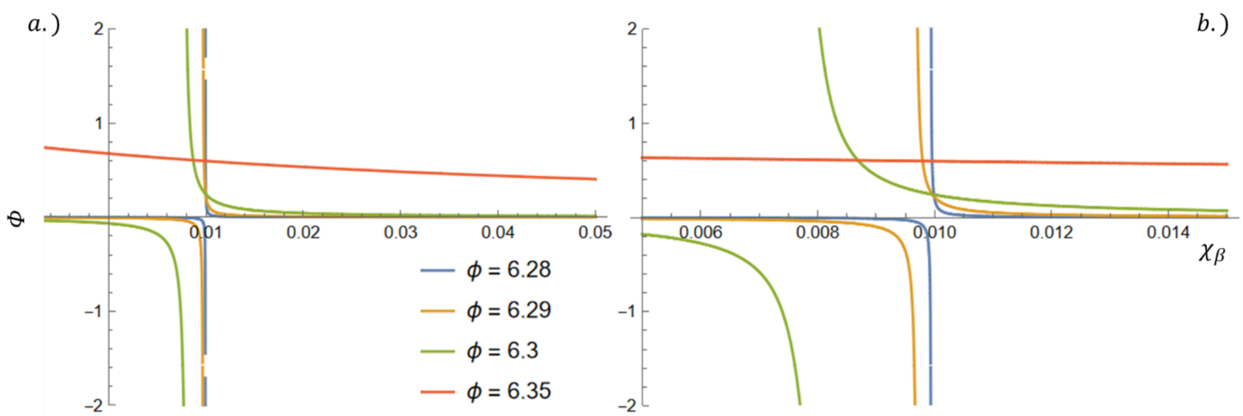

Figure 3.3 Φ against χ_β for various fixed ϕ

strongest nonlinearity (and thus most rapid phase flip) occurring at integer multiples of π and then slowest at odd multiples of π/2. However, as seen in Figure 3.4 a.), this is not necessarily the case, and some rather unexpected results were found. At ϕ = 7.85, or $\phi \approx (5/2)\pi$, the overall function does not diverge nearly as slowly at ϕ = 6.4, which is comparatively much closer to an integer multiple of π. By zooming in, Figure 3.4 b.) does reinforce the idea that when ϕ approaches an integer multiple of π, in this case 3π for ϕ = 9.42, the phase again flips rapidly.

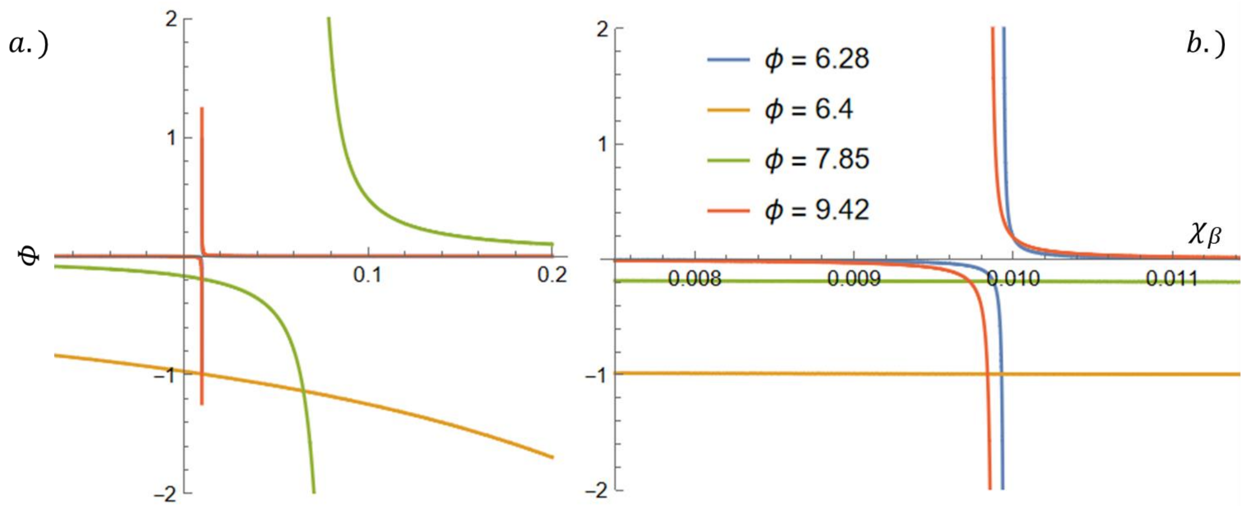

Figure 3.4 Unsuspected Φ against χ_β for various fixed ϕ

Plotting Φ for various values of ω' in Figure 3.5 a.) is somewhat striking in that it makes it obvious that for cases of $\omega' = \chi_\beta$ the function approaches the phase shift asymptotes. Here, the other values were set constant at $\phi = 6.28$ and $\gamma = 0.1$. Mathematically, full expansion of Equation 3.55 makes the plotted results pretty obvious in the case of $\phi = 6.28$, because the denominator of the total expression has multiplicative factors of $(\chi - \omega')$ and $(-1 + e^{2i\phi})$.

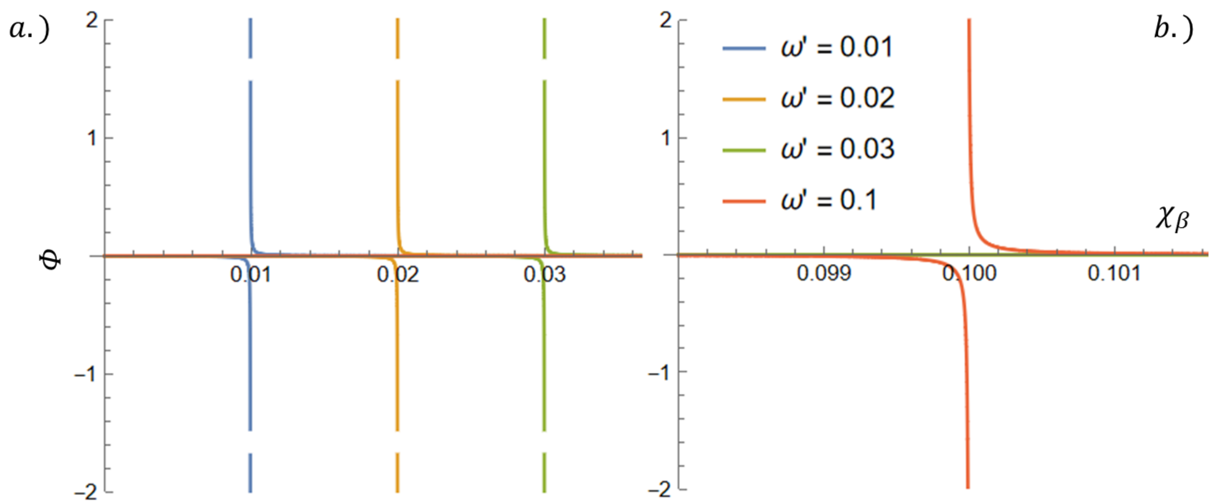

Figure 3.5 Φ against χ_β for various fixed ω'

Physically, however, it is somewhat surprising and seems to suggest a link between the detuning frequency and the exciton-exciton interaction energy. Additionally, in Figure 3.5 b.) the value of ω' has been raised to an order of magnitude higher than the previous values but Φ is still plotted on the same scale. While it does flip at a slower pace than the smaller values of ω', it is seen to have nowhere near as dramatic a shift for small changes to ϕ.

The final parameter investigated was the radiative decay rate of the exciton, γ, as shown in Figure 3.6. From a mathematical perspective, there was not much intuition for how changes in γ would affect Φ as its appearances in Equation 3.55 is rather complicated. The results, meanwhile, are crystal clear in that as γ increases the phase flip slows, implying a larger γ

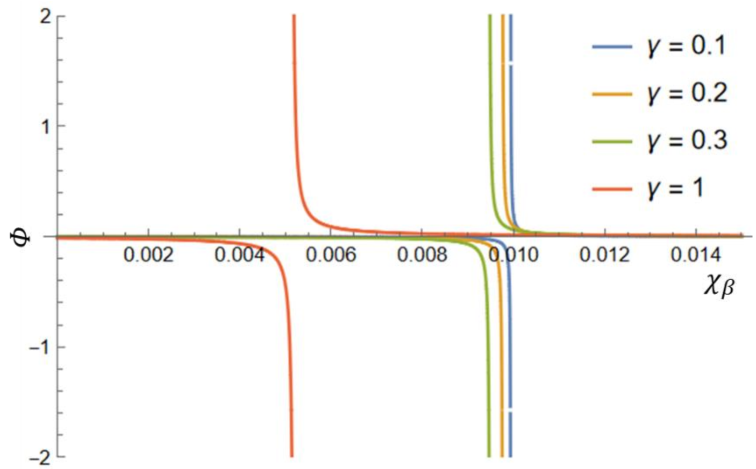

Figure 3.6 Φ against χ_β for various fixed γ

produces a lower nonlinear response. The inverse proportionality of $\gamma \propto 1/t_\gamma$, where t_γ is the radiative lifetime of the exciton. As the strength of the polariton is dependent upon its ability to oscillate between the photon and exciton substate, a larger γ (and thus small t_γ) enters further into the strong coupling regime (39). This was interpreted as a longer-lived exciton, in a polariton with an already heavily excitonic component, reduces the probability of the photon being radiated out of the cavity. It is worth noting that, in Figure 3.6, raising the value of γ an order of magnitude does indeed reduce the nonlinearity; the change in responses is like that of the frequency detuning seen in Figure 3.5 b.), where it can still be compared to smaller values on the same relative scale albeit flipping at a noticeably slower rate.

While these results are merely qualitative relationships, the physical implementation of these variables were then considered. The intrinsic values for a given TMD of many of these paramters vary extensively, and suggest high tunability for temperature, doping, strain, multilayer TMDs, heterostructure layering, an external dielectric environment, an applied potential, and dielectric screening from a substrate (39,40). Due to the nature of the tunability of ω' and ϕ by manually controlling the frequency of the incident light and the mechanical dimensions of the cavity, the limiting factors are the ability to modulate the interaction energy χ and the radiative rate γ of the excitons. As found in (35), such a system using MoSe2 ecapsulated in layers of hexagonal boron nitride can be made to have a linewidth as low as $\gamma \approx 0.8$ meV. As mentioned previously, there are continual discrepancies for consistent nonlinear responses in 2D TMDs, but there is much progress made in demonstrations of arbitrarily tuning the binding energies of the excitons (and thus the exciton-exciton interaction energy) (41,42).

Chapter 4: Results Discussion and Summary

Optical quantum bits present solutions to numerous issues that trouble more esoteric qubits, with the enormous caveat of their inability to interact with one another. Their potential for on-chip and room temperature quantum computing have driven researchers to continue searching for a photonic controlled-phase logic gate, U_{CP}, despite many dead-ends and set-backs. In this thesis, a solution for such a gate was proposed and investigated for proof-of-concept validity.

Inspired by the unique properties of an pseudo-Fabrey-Pérot resonator design discovered by Wild *et al* (23) and Zhou (35), a one-dimensional cavity consisting of a perfect reflecting boundary and a parallel atomically thin TMD was considered with two incident photons for feasibility as a U_{CP}. It was found that the TMD could enter a strong-coupling regime with two incident photons, generating a polariton with primarily excitonic degrees of freedom, trapping the photons within the resonator, and become a near-perfect mirror. This exciton-polariton phenomenon was then investigated for relationships between the frequency of the incident light, the radiative loss rates of its atomic constituents, the photonic phase operator accrual of traveling across the resonator, the coupling constant between the dipole excited state and the field state, and the excitonic interaction energy.

Nano- and microscale control of light frequency and cavity dimensions are commonplace. The ability to nudge the nonlinear response of monolayer TMDs on command has been heavily investigated in recent years. The physical engineering capabilities of realizing such a U_{CP} appear to either currently exist or may in the near future. There still requires investigation into the fidelity of encoded information interacting with the gate, as well as paring down experimental realizations for the various control parameters, but overall, the findings presented in this thesis cannot rule out a controlled phase gate of the proposed architecture.

Appendix A: MS Project

Fall 2019	**78 days**	**Mon 8/26/19**	**Wed 12/11/19**
Classes	**78 days**	**Mon 8/26/19**	**Wed 12/11/19**
Semiconductors	78 days	Mon 8/26/19	Wed 12/11/19
Quantum Mechanics	78 days	Mon 8/26/19	Wed 12/11/19
MEPH 5811	78 days	Mon 8/26/19	Wed 12/11/19
Physics 500V	78 days	Mon 8/26/19	Wed 12/11/19
Research	**78 days**	**Mon 8/26/19**	**Wed 12/11/19**
Read quantum optics book, literature	78 days	Mon 8/26/19	Wed 12/11/19
Spring 2020	**83 days**	**Mon 1/13/20**	**Wed 5/6/20**
Classes	**83 days**	**Mon 1/13/20**	**Wed 5/6/20**
Research Commercialization	83 days	Mon 1/13/20	Wed 5/6/20
Quantum Mechanics II	83 days	Mon 1/13/20	Wed 5/6/20
MEPH 6811	83 days	Mon 1/13/20	Wed 5/6/20
Research	**83 days**	**Mon 1/13/20**	**Wed 5/6/20**
Begin research	83 days	Mon 1/13/20	Wed 5/6/20
Summer 2020	**50 days**	**Mon 5/25/20**	**Fri 7/31/20**
Classes	**50 days**	**Mon 5/25/20**	**Fri 7/31/20**
Proposal and Grant Writing	50 days	Mon 5/25/20	Fri 7/31/20
Summer Research	**50 days**	**Mon 5/25/20**	**Fri 7/31/20**
Research with Dr. Gea-Banacloche	49 days	Tue 5/26/20	Fri 7/31/20
Fall 2020	**78 days**	**Fri 8/28/20**	**Tue 12/15/20**
Classes	**78 days**	**Fri 8/28/20**	**Tue 12/15/20**
MEMS	78 days	Fri 8/28/20	Tue 12/15/20
Condensed Matter	77 days	Fri 8/28/20	Mon 12/14/20
MEPH 5911	78 days	Fri 8/28/20	Tue 12/15/20
Fall Research	**78 days**	**Fri 8/28/20**	**Tue 12/15/20**
Research with Dr. Gea-Banacloche	78 days	Fri 8/28/20	Tue 12/15/20
Spring 2021	**82 days**	**Wed 1/13/21**	**Thu 5/6/21**
Classes	**82 days**	**Wed 1/13/21**	**Thu 5/6/21**
Electronic Packaging	82 days	Wed 1/13/21	Thu 5/6/21
Statistical Mechanics	82 days	Wed 1/13/21	Thu 5/6/21
MEPH 6911	82 days	Wed 1/13/21	Thu 5/6/21
Spring Research	**82 days**	**Wed 1/13/21**	**Thu 5/6/21**
Research with Dr. Gea-Banacloche	82 days	Wed 1/13/21	Thu 5/6/21
Summer 2021	**50 days**	**Mon 5/24/21**	**Fri 7/30/21**
Classes	**50 days**	**Mon 5/24/21**	**Fri 7/30/21**
Statistical Methods	50 days	Mon 5/24/21	Fri 7/30/21
Summer Research	**50 days**	**Mon 5/24/21**	**Fri 7/30/21**
Begin thesis writing	50 days	Mon 5/24/21	Fri 7/30/21
Research with Dr. Gea-Banacloche	50 days	Mon 5/24/21	Fri 7/30/21
Fall 2021	**85 days**	**Mon 8/23/21**	**Fri 12/17/21**
Classes	**85 days**	**Mon 8/23/21**	**Fri 12/17/21**
Electronic Packaging	85 days	Mon 8/23/21	Fri 12/17/21
Statistical Mechanics	85 days	Mon 8/23/21	Fri 12/17/21
Fall Research	**85 days**	**Mon 8/23/21**	**Fri 12/17/21**
Continue thesis writing	85 days	Mon 8/23/21	Fri 12/17/21
Clean-up and correct research	85 days	Mon 8/23/21	Fri 12/17/21
Spring 2022	**89 days**	**Tue 1/18/22**	**Fri 5/20/22**
Classes	**89 days**	**Tue 1/18/22**	**Fri 5/20/22**
Materials Characterization	89 days	Tue 1/18/22	Fri 5/20/22
Optoelectronics	89 days	Tue 1/18/22	Fri 5/20/22
Spring Research	**89 days**	**Tue 1/18/22**	**Fri 5/20/22**
Continue thesis writing	89 days	Tue 1/18/22	Fri 5/20/22
Continue clean-up and corrections	89 days	Tue 1/18/22	Fri 5/20/22
Summer 2022	**45 days**	**Mon 5/30/22**	**Fri 7/29/22**
Classes	**45 days**	**Mon 5/30/22**	**Fri 7/29/22**
Thesis Hours	45 days	Mon 5/30/22	Fri 7/29/22
Summer Research	**45 days**	**Mon 5/30/22**	**Fri 7/29/22**
Finish thesis writing	45 days	Mon 5/30/22	Fri 7/29/22
Finish clean-up and corrections	45 days	Mon 5/30/22	Fri 7/29/22
Summer 2022 Graduation	**45 days**	**Mon 5/30/22**	**Fri 7/29/22**
End Game	**45 days**	**Mon 5/30/22**	**Fri 7/29/22**
Apply for graduation	1 day	Fri 7/1/22	Fri 7/1/22
Final draft to Dr. Gea-Banacloche	1 day	Fri 7/8/22	Fri 7/8/22
Correction to final draft	6 days	Fri 7/8/22	Fri 7/15/22
Approval by professor	6 days	Fri 7/8/22	Fri 7/15/22
Send to committee	1 day	Fri 7/15/22	Fri 7/15/22
Approval by Dr. Leftwich	1 day	Mon 7/18/22	Mon 7/18/22
Last defense deadline	1 day	Mon 7/25/22	Mon 7/25/22
Final corrections	1 day	Fri 7/29/22	Fri 7/29/22
Deliver to grad school deadline	1 day	Fri 7/29/22	Fri 7/29/22

Appendix B: References

1. DiVincenzo DP. The Physical Implementation of Quantum Computation. Fortschritte Phys. 2000;48(9–11):771–83.

2. Michael A. Nielsen, Isaac L. Chuang. Quantum Computation and Quantum Information. 1st ed. New York, NY: Cambridge University Press; 2000.

3. Barenco A, Bennett CH, Cleve R, Divincenzo DP, Margolus N, Shor P, et al. Elementary gates for quantum computation. Phys Rev A. 1995;52(5):3457–67.

4. Shi Y. Both Toffoli and Controlled-NOT need little help to do universal quantum computation [Internet]. arXiv; 2002. Available from: https://arxiv.org/abs/quant-ph/0205115

5. Chuang IL, Yamamoto Y. A Simple Quantum Computer. Phys Rev A. 1995 Nov 1;52(5):3489–96.

6. Boyd RW, Prato D. Nonlinear Optics [Internet]. Elsevier Science; 2008. Available from: https://books.google.com/books?id=uoRUi1Yb7ooC

7. Rodney Loudon. The Quantum Theory of Light. London: Oxford University Press; 1973.

8. David N. Nikogosyan. Nonlinear Optical Crystals: A Complete Survey. New York, NY: Springer;

9. Shapiro JH. Single-photon Kerr nonlinearities do not help quantum computation. Phys Rev A. 2006 Jun;73(6):062305.

10. Gea-Banacloche J. Impossibility of large phase shifts via the giant Kerr effect with single-photon wave packets. Phys Rev A. 2010 Apr;81(4):043823.

11. Heuck M, Jacobs K, Englund DR. Controlled-Phase Gate Using Dynamically Coupled Cavities and Optical Nonlinearities. Phys Rev Lett. 2020 Apr 24;124(16):160501.

12. Li M, Zhang YL, Tang HX, Dong CH, Guo GC, Zou CL. Photon-Photon Quantum Phase Gate in a Photonic Molecule with $\ensuremath\chi^(2)$ Nonlinearity. Phys Rev Appl. 2020 Apr;13(4):044013.

13. Niu MY, Chuang IL, Shapiro JH. Qudit-Basis Universal Quantum Computation Using χ^{(2)} Interactions. Phys Rev Lett. 2018 Apr 20;120(16):160502.

14. Krastanov S, Heuck M, Shapiro JH, Narang P, Englund DR, Jacobs K. Room-temperature photonic logical qubits via second-order nonlinearities. Nat Commun. 2021 Jan 8;12(1):191.

15. Mak KF, Lee C, Hone J, Shan J, Heinz TF. Atomically thin MoS 2: a new direct-gap semiconductor. Phys Rev Lett. 2010;105(13):136805.

16. Novoselov KS, Mishchenko A, Carvalho A, Neto AHC. 2D materials and van der Waals heterostructures. Science. 2016;353(6298):aac9439.

17. Chowdhury T, Sadler EC, Kempa TJ. Progress and Prospects in Transition-Metal Dichalcogenide Research Beyond 2D. Chem Rev. 2020 Nov 25;120(22):12563–91.

18. Wang QH, Kalantar-Zadeh K, Kis A, Coleman JN, Strano MS. Electronics and optoelectronics of two-dimensional transition metal dichalcogenides. Nat Nanotechnol. 2012 Nov 1;7(11):699–712.

19. Kuc A, Zibouche N, Heine T. Influence of quantum confinement on the electronic structure of the transition metal sulfide TS2. Phys Rev B. 2011 Jun;83(24):245213.

20. Schneider C, Glazov MM, Korn T, Höfling S, Urbaszek B. Two-dimensional semiconductors in the regime of strong light-matter coupling. Nat Commun. 2018 Jul 12;9(1):2695.

21. Ugeda MM, Bradley AJ, Shi SF, da Jornada FH, Zhang Y, Qiu DY, et al. Giant bandgap renormalization and excitonic effects in a monolayer transition metal dichalcogenide semiconductor. Nat Mater. 2014 Dec;13(12):1091–5.

22. Wang G, Chernikov A, Glazov MM, Heinz TF, Marie X, Amand T, et al. Colloquium: Excitons in atomically thin transition metal dichalcogenides. Rev Mod Phys. 2018 Apr;90(2):021001.

23. Wild DS, Shahmoon E, Yelin SF, Lukin MD. Quantum Nonlinear Optics in Atomically Thin Materials. Phys Rev Lett. 2018 Sep;121(12):123606.

24. Fan Z, Geng Z, Fang W, Lv X, Su Y, Wang S, et al. Characteristics of transition metal dichalcogenides in optical pumped modulator of terahertz wave. AIP Adv. 2020;10(4):045304.

25. Malard LM, Alencar TV, Barboza APM, Mak KF, de Paula AM. Observation of intense second harmonic generation from MoS$_2$ atomic crystals. Phys Rev B. 2013 May;87(20):201401.

26. Janisch C, Wang Y, Ma D, Mehta N, Elías AL, Perea-López N, et al. Extraordinary Second Harmonic Generation in tungsten disulfide monolayers. Sci Rep. 2014 Jul 2;4:5530.

27. Ribeiro-Soares J, Janisch C, Liu Z, Eli\’as AL, Dresselhaus MS, Terrones M, et al. Second Harmonic Generation in WSe2. 2D Mater. 2015 Dec;2(4):045015.

28. Chen H, Corboliou V, Solntsev AS, Choi DY, Vincenti MA, Ceglia D de, et al. Enhanced second-harmonic generation from two-dimensional MoSe2 by waveguide integration. 2017 Conf Lasers Electro-Opt CLEO. 2017;1–2.

29. Beams R, Cançado LG, Krylyuk S, Kalish I, Kalanyan B, Singh AK, et al. Characterization of Few-Layer 1T’ MoTe(2) by Polarization-Resolved Second Harmonic Generation and Raman Scattering. ACS Nano. 2016 Oct 25;10(10):9626–36.

30. Ye Z, Cao T, O’Brien K, Zhu H, Yin X, Wang Y, et al. Probing excitonic dark states in single-layer tungsten disulphide. Nature. 2014 Sep 1;513(7517):214–8.

31. Regan EC, Wang D, Paik EY, Zeng Y, Zhang L, Zhu J, et al. Emerging exciton physics in transition metal dichalcogenide heterobilayers. Nat Rev Mater [Internet]. 2022 May 4; Available from: https://doi.org/10.1038/s41578-022-00440-1

32. Shayeganfar F. Strain engineering of electronic properties and anomalous valley hall conductivity of transition metal dichalcogenide nanoribbons. Sci Rep. 2022 Jul 4;12(1):11285.

33. Bilc DI, Benea D, Pop V, Ghosez P, Verstraete MJ. Electronic and Thermoelectric Properties of Transition-Metal Dichalcogenides. J Phys Chem C. 2021 Dec 16;125(49):27084–97.

34. Shahmoon E, Wild DS, Lukin MD, Yelin SF. Cooperative Resonances in Light Scattering from Two-Dimensional Atomic Arrays. Phys Rev Lett. 2017 Mar;118(11):113601.

35. Zhou Y, Scuri G, Sung J, Gelly RJ, Wild DS, De Greve K, et al. Controlling Excitons in an Atomically Thin Membrane with a Mirror. Phys Rev Lett. 2020 Jan;124(2):027401.

36. Bettles RJ, Gardiner SA, Adams CS. Enhanced Optical Cross Section via Collective Coupling of Atomic Dipoles in a 2D Array. Phys Rev Lett. 2016 Mar;116(10):103602.

37. Hoi IC, Kockum AF, Tornberg L, Pourkabirian A, Johansson G, Delsing P, et al. Probing the quantum vacuum with an artificial atom in front of a mirror. Nat Phys. 2015 Dec 1;11(12):1045–9.

38. Tassone F, Yamamoto Y. Exciton-exciton scattering dynamics in a semiconductor microcavity and stimulated scattering into polaritons. Phys Rev B. 1999 Apr;59(16):10830–42.

39. Palummo M, Bernardi M, Grossman JC. Exciton radiative lifetimes in two-dimensional transition metal dichalcogenides. Nano Lett. 2015 May 13;15(5):2794–800.

40. Rivera P, Schaibley JR, Jones AM, Ross JS, Wu S, Aivazian G, et al. Observation of long-lived interlayer excitons in monolayer MoSe2–WSe2 heterostructures. Nat Commun. 2015 Feb 24;6(1):6242.

41. Strikha MV, Kurchak AI, Morozovska AN. Gate-Voltage Control of Quantum Yield in Monolayer Transition-Metal Dichalcogenide. Phys Rev Appl. 2020 Jan;13(1):014040.

42. Wang Y, Xiao J, Chung TF, Nie Z, Yang S, Zhang X. Direct electrical modulation of second-order optical susceptibility via phase transitions. Nat Electron. 2021 Oct 1;4(10):725–30.